

DOI: 10.1002/cbic.201000692

## Intense Blue Fluorescence in a Leucine Zipper Assembly

Hiroshi Tsutsumi,<sup>[a, c]</sup> Seiichiro Abe,<sup>[a, b]</sup> Tomoaki Mino,<sup>[a, b]</sup> Wataru Nomura,<sup>[a]</sup> and Hirokazu Tamamura<sup>\*[a, b]</sup>

Fluorescent probes are valuable molecular tools in chemical biology, and various fluorescent probes for the detection of small biological components have been developed and used for fluorescence imaging in cells.<sup>[1]</sup> Ratiometric fluorescent probes and fluorogenic probes are particularly useful because they can suppress noise associated with background emission.<sup>[2]</sup> Tag/probe pairs for the fluorescence imaging of proteins have recently been developed,<sup>[3]</sup> but the number of fluorogenically active tag/probe pairs is still limited.

Green fluorescent protein (GFP) is a widely used biological tool for the imaging of proteins in live cells.<sup>[4]</sup> Its fluorescence is well controlled because the fluorophore unit is located in a unique microenvironment inside a  $\beta$ -barrel structure. We have previously developed a new tag/probe pair with fluorogenic activity—based on the unique characteristics of GFP—by use of the leucine zipper assembly, the ZIP tag/probe.<sup>[5]</sup> The environment surrounding the 4-nitrobenzo-2-oxa-1,3-diazole (NBD) component of the probe peptide changes drastically from a hydrophilic state to a hydrophobic state through the formation of a  $3\alpha$ -helical leucine zipper structure between the tag and the probe peptides, as a result of which the bright green fluorescence of the NBD dye is induced. Use of other solvatochromic fluorophores should enable us to develop fluorogenic ZIP tag/probe pairs with other fluorescence colors. Here we describe the use of 7-diethylaminocoumarin-3-carboxylic acid (DEAC) in the development of another ZIP tag/probe pair with switchable blue fluorescence.

ZIP tag/probe pairs containing the DEAC dye were designed as described in our previous report (Scheme 1).<sup>[5]</sup> In a probe  $\alpha$ -helical peptide, a DEAC moiety was attached to the side chain of L- $\alpha$ -2,3-diaminopropionic acid [Dap(DEAC)]. A Dap(DEAC) residue is situated at the X-position in the probe peptide to locate the DEAC dye in the hydrophobic region of the  $3\alpha$ -helical leucine zipper structure. In tag antiparallel  $2\alpha$ -helical peptides, two Leu residues at the Z-positions in the L2 peptide are residues complementary to the Dap(DEAC) residue of the

probe peptide, and these residues are replaced by alanine (A2 peptide) or glycine (G2 peptide) so that hydrophobic spaces can be formed when the tag peptides bind to the probe peptide.

The fluorescence spectra of the DEAC probe peptide showed a remarkable change as the concentration of the A2 peptide was increased. The emission maximum due to the DEAC dye shifted from 482 to 470 nm as the emission intensity increased (Figure 1B). A DEAC- $\beta$ -alanine methyl ester (**7**) showed emission maxima at 483 nm in HEPES buffer solution and at 470 nm in MeOH (see the Supporting Information). These results clearly suggest that through the formation of the DEAC probe/A2 peptide complex, the DEAC moiety of the probe peptide is moved from a hydrophilic environment in bulk water to a hydrophobic environment inside the  $3\alpha$ -helical bundle structure. The fluorescence intensity of the DEAC probe peptide at 470 nm increased up to 10.5 times on addition of A2 in a typical saturation manner (Figure 2A, Table 1).

**Table 1.** Emission maxima,  $\Delta I_{\max}/I_0$  values (in parentheses), and relative fluorescent quantum yields of the probe peptide and tag/probe complexes, the dissociation constants ( $K_d$ ) between the tag and the probe peptides, and the  $\alpha$ -helical contents of the probe, the tag peptides, and their complexes (in parentheses).

	Probe	L2	A2	G2
$\lambda_{\max}$ ( $\Delta I_{\max}/I_0$ )	482 nm (-)	466 nm (3.4)	470 nm (10.5)	457 nm (51.7)
$\phi_f^{[a]}$	1	5.56	17.7	39.2
$K_d^{[b]}$	-	94.0 nM <sup>[d]</sup>	2.29 nM <sup>[e]</sup>	250 nM <sup>[f]</sup>
$\alpha$ -helix content <sup>[c]</sup>	60%	81% (78%)	58% (76%)	19% (72%)

[a] Relative fluorescent quantum yield at 430 nm excitation. [b] Measurement conditions: HEPES buffer solution [pH 7.2, 50 mM, NaCl (100 mM)], 25 °C, [probe] = 0.5  $\mu$ M. [c] Measurement conditions: Tris-HCl buffer solution [pH 7.2, 50 mM, NaCl (100 mM)], 25 °C, [tag], [probe], [tag/probe] = 1.0  $\mu$ M. The  $\alpha$ -helical contents were determined by a standard method. [d]–[f] Determined from the fluorescent intensity changes at 466, 470, or 457 nm, respectively.

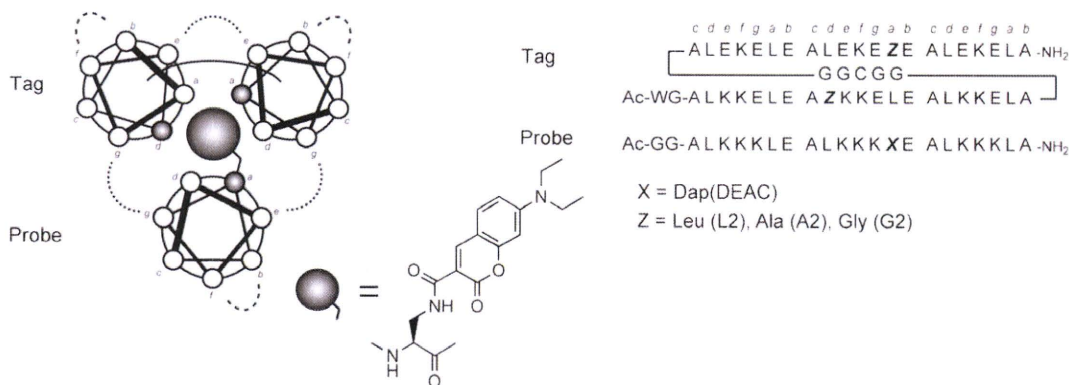
[a] Dr. H. Tsutsumi, S. Abe, T. Mino, Dr. W. Nomura, Prof. H. Tamamura  
Institute of Biomaterials and Bioengineering  
Tokyo Medical and Dental University  
Chiyoda-ku, Tokyo 101-0062 (Japan)

[b] S. Abe, T. Mino, Prof. H. Tamamura  
School of Biomedical Science, Tokyo Medical and Dental University  
Chiyoda-ku, Tokyo 101-0062 (Japan)  
Fax: (+81) 3-5280-8039  
E-mail: tamamura.mr@tmd.ac.jp

[c] Dr. H. Tsutsumi  
Present address: Department of Synthetic Chemistry and  
Biological Chemistry, Graduate School of Engineering  
Kyoto University Katsura  
Kyoto, 615-8510 (Japan)

Supporting information for this article is available on the WWW under  
<http://dx.doi.org/10.1002/cbic.201000692>.

The fluorescent intensity of the DEAC probe/A2 peptide complex at 470 nm is about eight times higher than that of compound **7** in MeOH and the complex showed a similar fluorescent spectrum to that of compound **7** in acetone. These results indicate that the microenvironment in the DEAC probe/A2 peptide complex might be more hydrophobic than MeOH. The shift of the emission maximum of the L2 peptide, from 482 to 466 nm, was slightly larger than that of the DEAC probe/A2 peptide pair, but the fluorescence intensity change was lower than that in the case of the A2 peptide (3.4 times at 466 nm; Figure 1A, Table 1). This result implies that the small fluorescent change in the DEAC probe/L2 peptide complex might be



Scheme 1. Structures and amino acid sequences of ZIP tag/probe pairs containing DEAC dye.

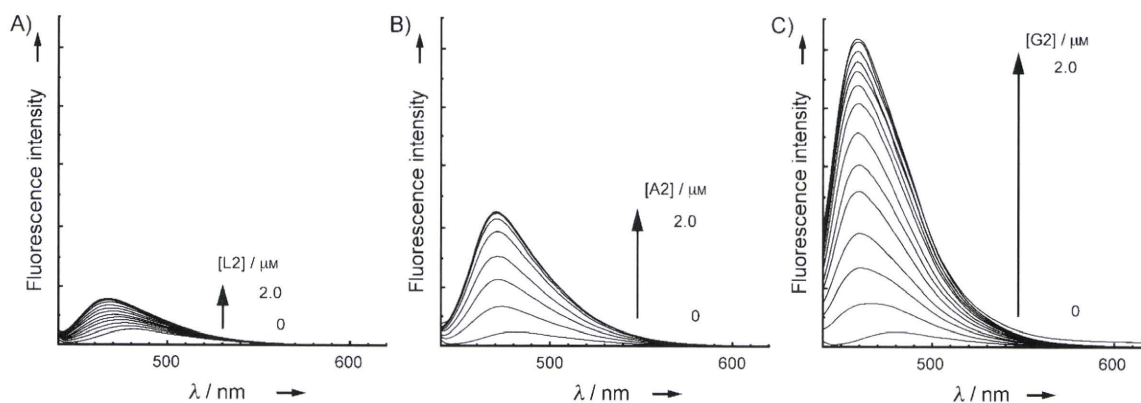


Figure 1. Fluorescence spectral change of the DEAC probe peptide upon addition of A) L2, B) A2, and C) G2 at 25 °C in HEPES buffer [pH 7.2, 50 mM, NaCl (100 mM)]: [probe] = 0.5 μM,  $\lambda_{\text{ex}}$  = 430 nm.

caused by a lack of space to accommodate the DEAC dye. Interestingly, the addition of the G2 peptide to the DEAC probe peptide induced a significant blue shift, from 482 nm to

457 nm in the emission maximum and a substantial enhancement of the fluorescent intensity at 457 nm (51.7 times; Figure 2A, Table 1). The fluorescent spectrum of the DEAC probe/G2 peptide complex is similar to that of compound 7 in dichloromethane (Figure S1 in the Supporting Information). These results indicate that the DEAC dye is located in an extremely hydrophobic environment in the DEAC probe/G2 peptide complex. The relative fluorescent quantum yields ( $\phi_r$ ) of the DEAC probe/A2 peptide pair and the DEAC probe/G2 peptide pair relative to the probe peptide alone are 17.7 and 39.2, respectively (Table 1). Although fluorescent quantum yields of DEAC dye derivatives in aqueous media are low,<sup>[6]</sup> these remarkable  $\phi_r$  increases enable the naked eye to detect the fluorescent change (Figure 2B).

In the circular dichroism (CD) study, the L2, A2, and DEAC probe peptides showed CD spectral patterns typical of  $\alpha$ -helical structures, with negative maxima at 208 and 222 nm, whereas the G2 peptide, in contrast, showed a random coil pattern (Figure 3). The  $\alpha$ -helical contents of L2, A2, G2, and the DEAC probe peptides were determined to be 81, 58, 19, and 60%, respectively, by a standard method (Table 1).<sup>[7]</sup> The  $\alpha$ -helical content of the DEAC probe peptide/A2 complex is estimated as 76%, which is higher than those of the DEAC probe pep-

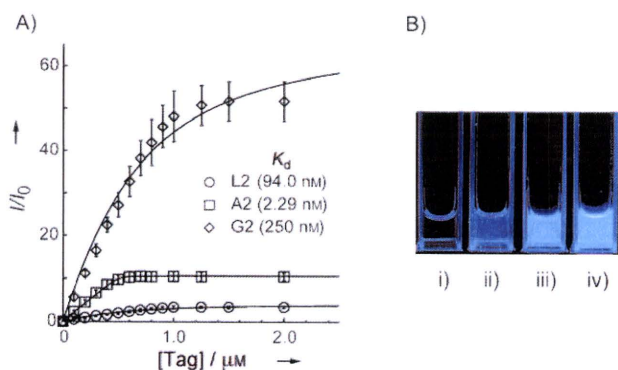
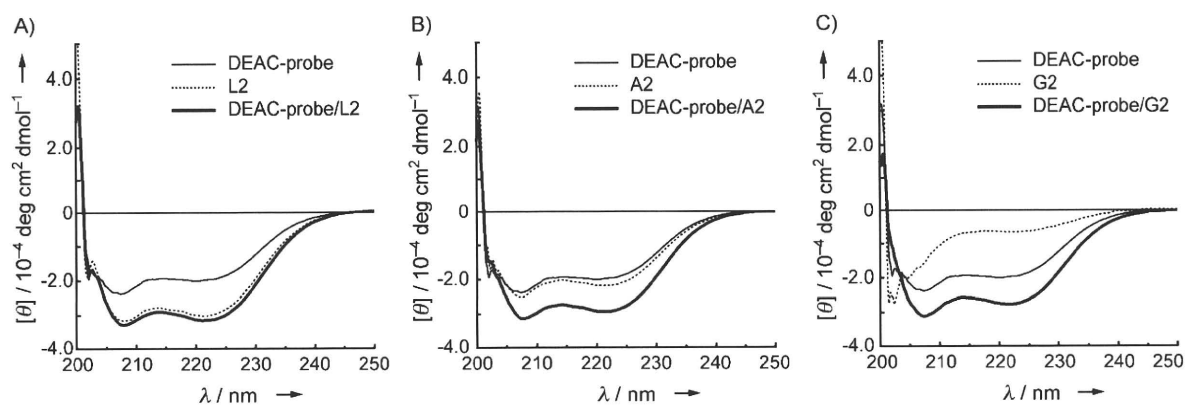


Figure 2. A) Fluorescence titration curves of the DEAC probe peptide with L2, A2, and G2 at 466, 470, and 457 nm, respectively.  $I$  represents the fluorescent intensity at various concentrations of tag peptides and  $I_0$  the initial fluorescent intensity. B) Fluorescent photography of: i) the DEAC probe peptide, ii) the DEAC probe peptide/L2 complex, iii) the DEAC probe peptide/A2 complex, and iv) the DEAC probe peptide/G2 complex. [Probe] = 0.5 μM, [tag] = 2.0 μM.



**Figure 3.** Circular dichroism spectra of tag and the DEAC probe peptides at 25°C in Tris-HCl buffer [pH 7.2, 50 mM, NaCl (100 mM)]. A) The DEAC probe peptide (solid line), L2 (dashed line), and the complex of probe/L2 (bold solid line). B) The DEAC probe peptide (solid line), A2 (dashed line), and the complex of probe/A2 (bold solid line). C) The DEAC probe peptide (solid line), G2 (dashed line), and the complex of probe/G2 (bold solid line).

ptide or the A2 peptide alone, suggesting that more stable  $\alpha$ -helical structures are induced in the DEAC probe/A2 peptide complex through the formation of the 3 $\alpha$ -helical leucine zipper structure. Enhancement of the  $\alpha$ -helical structure of the DEAC probe peptide was also observed in the DEAC probe/L2 peptide complex, with an  $\alpha$ -helical content of 78%. Interestingly, a similar enhancement of  $\alpha$ -helical structure was observed in the DEAC probe/G2 peptide complex (72%) but the  $\alpha$ -helical content of the G2 peptide was only 19%. The G2 peptide has two glycine residues, which destabilize  $\alpha$ -helix structures generally, and this is presumably the reason for its lower  $\alpha$ -helix content. On the other hand, the G2 peptide might easily be folded into a stable  $\alpha$ -helical structure by complexation with the DEAC probe peptide in the induced fit manner. This result clearly suggests that the DEAC probe/G2 peptide pair can also form a stable 3 $\alpha$ -helical structure. The shape of the hydrophobic space formed in the DEAC probe/G2 peptide complex might fit well to the DEAC dye and as a result, the DEAC dye would be tightly fixed in the hydrophobic space and the bright blue fluorescence would result.

The apparent dissociation constants ( $K_d$ ) of the DEAC peptide with the L2, A2, and G2 peptides were determined to be 93.9 nM, 2.29 nM, and 250 nM, respectively, by a nonlinear least-squares curve fitting method based on a 1:1 stoichiometry model<sup>[8]</sup> (Table 1), and so the binding affinities of the L2 and A2 peptides for the DEAC probe peptide were higher than that of the G2 peptide. The L2 and A2 peptides showed high  $\alpha$ -helix contents before complexation with the DEAC probe peptide, but the G2 peptide, in contrast, showed a random coil structure. These results suggest that the prefolded  $\alpha$ -helix structure of the L2 and A2 peptides is important for the high-affinity binding to the DEAC probe peptide. However, the binding affinity between the G2 peptide and the DEAC probe peptide is thought to be sufficiently strong as a tag/probe pair for protein labeling. In addition, a cross-linking strategy might be useful to compensate the binding affinity of the G2 peptide and the DEAC probe peptide. We have recently reported cross-link-type ZIP tag/probe pairs based on covalent bond forma-

tion that enhances the binding affinities and the complex stabilities of tag probe pairs.<sup>[5b]</sup>

In conclusion, we have developed leucine zipper tag/probe pairs with blue fluorogenic activity. The weak fluorescence seen in the DEAC probe peptide alone is greatly intensified through binding with the A2 or G2 tag peptides. In particular, the G2 peptide induces a greater than 50-fold fluorescence enhancement of the DEAC probe peptide concurrently with a large blue shift of the emission maximum. The G2 peptide binds to the DEAC probe peptide in an induced fit manner, which appears to be essential for the remarkable fluorescent change. The fluorescence enhancement of the DEAC probe peptide induced by the binding to the A2 and G2 peptides can easily be detected by the naked eye. Pairs of the DEAC probe peptide and the A2 or G2 peptides are thus new ZIP tag/probe pairs with blue turn-on fluorescence.

**Keywords:** coumarin • fluorescence • imaging agents • leucine zipper • peptides

- [1] a) *Topics in Fluorescence Spectroscopy, Vol. 9: Advanced Concepts in Fluorescence Sensing, Part A: Small Molecule Sensing* (Eds.: C. D. Geddes, J. R. Lakowicz), Springer, New York, 2005; b) *Topics in Fluorescence Spectroscopy, Vol. 10: Advanced Concepts in Fluorescence Sensing, Part B: Macromolecular Sensing* (Eds.: C. D. Geddes, J. R. Lakowicz), Springer, New York, 2005.
- [2] a) T. Terai, T. Nagano, *Curr. Opin. Chem. Biol.* **2008**, *12*, 515–521; b) G. Gryniewicz, M. Poenie, R. Y. Tsien, *J. Biol. Chem.* **1985**, *260*, 3440–3450; c) A. Ojida, I. Takashima, T. Kohira, H. Nonaka, I. Hamachi, *J. Am. Chem. Soc.* **2008**, *130*, 12095–12101.
- [3] a) B. A. Griffin, S. R. Adams, R. Y. Tsien, *Science* **1998**, *281*, 269–272; b) E. G. Guignet, R. Hovius, H. Vogel, *Nat. Biotechnol.* **2004**, *22*, 440–444; c) A. Ojida, K. Honda, D. Shinmi, S. Kiyonaka, Y. Mori, I. Hamachi, *J. Am. Chem. Soc.* **2006**, *128*, 10452–10459; d) A. Keppler, S. Gendreizig, T. Gronemeyer, H. Pick, H. Vogel, K. Johnsson, *Nat. Biotechnol.* **2002**, *21*, 86–89; e) K. Stöhr, D. Sieberg, T. Ehrhard, K. Lympelopoulou, S. Öz, S. Schulmeister, A. C. Pfeifer, J. Bachmann, U. Klingmüller, V. Sourjik, D.-P. Herten, *Anal. Chem.* **2010**, *82*, 8186–8193; f) G. V. Los, A. Dazins, N. Karassina, C. Zimprich, M. G. McDougall, L. P. Encell, R. Friedman-Ohana, M. Wood, G. Vidurjiris, *Promega Cell Notes* **2005**, *11*, 2–6; g) S. Mizukami, S. Watanabe, Y. Hori, K. Kikuchi, *J. Am. Chem. Soc.* **2009**, *131*, 5016–5017.

- [4] a) O. Shimomura, F. H. Johnson, Y. Saiga, *J. Cell. Comp. Physiol.* **1962**, *59*, 223–229; b) M. Zimmer, *Chem. Rev.* **2002**, *102*, 759–781; c) R. Y. Tsien, *FEBS Lett.* **2005**, *579*, 927–932.
- [5] a) H. Tsutsumi, W. Nomura, S. Abe, T. Mino, A. Masuda, N. Ohashi, T. Tanaka, K. Ohba, N. Yamamoto, K. Akiyoshi, H. Tamamura, *Angew. Chem.* **2009**, *121*, 9328–9330; *Angew. Chem. Int. Ed.* **2009**, *48*, 9164–9166; b) W. Nomura, T. Mino, T. Narumi, N. Ohashi, A. Masuda, C. Hashimoto, H. Tsutsumi, H. Tamamura, *Biopolymers* **2010**, *94*, 843–852.
- [6] K. Azuma, S. Suzuki, S. Uchiyama, T. Kajiro, T. Santa, K. Imai, *Photochem. Photobiol. Sci.* **2003**, *2*, 443–449.
- [7] D. Y. Jackson, D. S. King, J. Chmielewski, S. Singh, P. G. Schultz, *J. Am. Chem. Soc.* **1991**, *113*, 9391–9392.
- [8] T. Kuwabara, A. Nakamura, A. Ueno, F. Toda, *J. Phys. Chem.* **1994**, *98*, 6297–6303.

---

Received: November 15, 2010

Published online on February 8, 2011

## Fluorescent-Responsive Synthetic C1b Domains of Protein Kinase C $\delta$ as Reporters of Specific High-Affinity Ligand Binding

Nami Ohashi,<sup>†</sup> Wataru Nomura,<sup>\*,†</sup> Tetsuo Narumi,<sup>†</sup> Nancy E. Lewin,<sup>‡</sup> Kyoko Itotani,<sup>†</sup> Peter M. Blumberg,<sup>‡</sup> and Hirokazu Tamamura<sup>\*,†</sup>

Department of Medicinal Chemistry, Institute of Biomaterials and Bioengineering, Tokyo Medical and Dental University, 2-3-10 Kandasurugadai, Chiyoda-ku, Tokyo 101-0062, Japan, and Laboratory of Cancer Biology and Genetics, Center for Cancer Research, National Cancer Institute, National Institutes of Health, Bethesda, Maryland 20892, United States. Received September 18, 2010; Revised Manuscript Received December 3, 2010

Protein kinase C (PKC) is a critical cell signaling pathway involved in many disorders such as cancer and Alzheimer-type dementia. To date, evaluation of PKC ligand binding affinity has been performed by competitive studies against radiolabeled probes that are problematic for high-throughput screening. In the present study, we have developed a fluorescent-based binding assay system for identifying ligands that target the PKC ligand binding domain (C1 domain). An environmentally sensitive fluorescent dye (solvatochromic fluorophore), which has been used in multiple applications to assess protein-binding interactions, was inserted in proximity to the binding pocket of a novel PKC $\delta$  C1b domain. These resultant fluorescent-labeled  $\delta$ C1b domain analogues underwent a significant change in fluorescent intensity upon ligand binding, and we further demonstrate that the fluorescent  $\delta$ C1b domain analogues can be used to evaluate ligand binding affinity.

### INTRODUCTION

Protein kinase C (PKC) is a family of serine/threonine protein kinases comprising 11 isozymes divided into three subclasses, termed conventional ( $\alpha$ ,  $\beta_{I/II}$ ,  $\gamma$ ), novel ( $\delta$ ,  $\epsilon$ ,  $\eta$ ,  $\theta$ ), and atypical ( $\zeta$ ,  $\lambda$ ,  $\iota$ ). Their classification is based on their essential structures and affinities for regulatory factors such as diacylglycerol (DAG) and calcium that bind to the C1 and C2 domains, respectively, of PKC. PKC plays a pivotal role in physiological responses to growth factors, oxidative stress, and tumor promoters (phorbol esters). These responses regulate numerous cellular processes (1, 2), including proliferation (3), differentiation (4), migration (5), and apoptosis (6, 7). The extensive involvement of PKC in both normal physiology and in numerous disorders has caused PKC to emerge as an important therapeutic target (8–10). Since PKC activation is regulated through the binding of ligands to its C1 domains, development of useful ligands targeted to the C1 domains has been of intense interest for medicinal chemists. Various synthetic PKC ligands based on  $\gamma$ -lactone templates have been developed and evaluated (11–13). On the other hand, since structures of many of the potent, naturally occurring PKC ligands such as the phorbol esters are highly complex, it has been difficult to extensively probe their structure–activity relationships. Much opportunity therefore remains for the development of ligands optimized for isozyme selectivity or other properties. Fluorescent-based methods possess many advantages for high-throughput screening. Especially, utilization of environmentally sensitive fluorophores is suitable for high-throughput techniques because washing steps are not generally required. Fluorophores often respond to the environmental changes in hydrophobic/hydrophilic states associated with the conformational changes of proteins accompanying ligand binding. Several screening methods based on fluorescent-modified

peptides, e.g., an IP<sub>3</sub> sensor, have been developed to date (14–17). In this study, fluorescent-labeled C1b domains of PKC $\delta$  utilizing a solvatochromic dye as a sensor of ligand binding were designed and synthesized as efficient screening tools to evaluate ligand binding and to explore novel PKC pharmacophores.

### EXPERIMENTAL PROCEDURES

**General Methods.** For chromatography, Wakogel C-200 (Wako Pure Chemical Industries, Ltd.) was employed. <sup>1</sup>H NMR and <sup>13</sup>C NMR spectra were recorded using a Bruker Ultrashield Plus Avance 400 spectrometer. Relative chemical shifts were reported in  $\delta$  (ppm) in DMSO-*d*<sub>6</sub> or in CDCl<sub>3</sub> with tetramethylsilane as an internal standard. Low- and high-resolution mass spectra were recorded on a JMS-T1000LC AccuTOF and Bruker Daltonics microTOF-2focus. RP-HPLC was performed with linear gradients of acetonitrile and H<sub>2</sub>O containing 0.1% (v/v) TFA (column: Cosmosil  $\mu$ C<sub>18</sub> AR-II (4.6  $\times$  250 mm) for analytical runs, Cosmosil  $\mu$ C<sub>18</sub> AR-II (20  $\times$  250 mm) for preparative runs. UV absorbance spectra were recorded on a Jasco V-650 spectrophotometer using a 1.0 cm path length quartz cuvette. Fluorescent spectra were recorded on a Jasco FP-6600 spectrofluorometer using a 1.0 cm path length quartz cuvette. Measurements of fluorescent intensity on 96-well plates were performed on a Wallac ARVO MX (Perkin-Elmer).

**Peptide Synthesis.** The protected peptide of  $\delta$ C1b(247–281) was manually constructed on a Novasyn TGR resin (0.25 mmol/g) by standard Fmoc-based solid phase peptide synthesis (SPPS). Fmoc-protected amino acid derivatives (5 equiv) were successively condensed using 1,3-diisopropylcarbodiimide (DIPCI) (5 equiv) in the presence of 1-hydroxybenzotriazole  $\cdot$  H<sub>2</sub>O (HOBt  $\cdot$  H<sub>2</sub>O) (5 equiv) in DMF (2 mL) (90 min treatment). The following side-chain protecting groups were used: Boc for Lys; Pbf for Arg; OBU' for Asp; Trt for Asn, Cys, and His; Bu' for Ser, Thr, and Tyr. The Fmoc group was deprotected with 20% (v/v) piperidine in DMF (2 mL) for 15 min. The resulting protected peptide was cleaved from the resin and deprotected with TFA-thioanisole-*m*-cresol-triisopropylsilane (TIS) (89:7.5:2.5:1, v/v) (90 min treatment). Deprotected peptides were

\* To whom correspondence should be addressed. E-mail: nomura.mr@tmd.ac.jp; tamamura.mr@tmd.ac.jp. Phone: +81-3-5280-8036. Fax: +81-3-5280-8039.

<sup>†</sup> Tokyo Medical and Dental University.

<sup>‡</sup> National Institutes of Health.

washed with cold Et<sub>2</sub>O three times. The product was then purified by RP-HPLC. The protected peptides of dansyl-labeled  $\delta$ C1b(221–246) were manually elongated on an Fmoc-His(Trt)-Trt(2-Cl)-resin (0.42 mmol/g) by Fmoc-based SPPS as in the synthesis of  $\delta$ C1b(247–281). The following side-chain protecting groups were used: Boc for Lys; Pbf for Arg; OBu' for Asp, Glu; Trt for Asn, Cys, Gln, and His; Bu' for Ser, Thr, and Tyr. At the dansyl-labeled position, Fmoc-Lys(DnsGly)-OH was used. The resulting protected peptides were cleaved from the resin with trifluoroethanol (TFE)-AcOH-DCM (1:1:3, v/v) (2 h treatment), followed by thioesterification. Deprotection was performed as in the synthesis of  $\delta$ C1b(247–281). The product was then purified by RP-HPLC. Mass data and chemical yields of these peptides are described in Supporting Information.

**Thioesterification.** Thioesterification was performed with ethyl mercaptopropionate (20 equiv), HOBt·H<sub>2</sub>O (10 equiv), and 1-(3-dimethylaminopropyl)-3-ethylcarbodiimide (EDCI)·HCl (10 equiv) in DMF (1 mL) (–20 °C, overnight). DMF was removed by evaporation, and the crude products were washed with H<sub>2</sub>O.

**Native Chemical Ligation.** Dansyl-labeled  $\delta$ C1b(221–246) (1.8 mg, 0.5  $\mu$ mol) and the  $\delta$ C1b(247–281) (1.9 mg, 0.5  $\mu$ mol) were dissolved in 500  $\mu$ L of 100 mM phosphate buffer (pH 8.5) containing 6 M guanidine hydrochloride (Gn·HCl) containing 2 mM EDTA and tris(2-carboxyethyl)phosphine hydrochloride (TCEP·HCl) (1.4 mg, 5  $\mu$ mol). Thiophenol (15 mL, 3%) was then added to the mixture. The ligation reaction was performed at 37 °C under an N<sub>2</sub> atmosphere. Progress of the ligation reaction was monitored by RP-HPLC (gradient: 25–45% of acetonitrile/0.1% TFA against H<sub>2</sub>O/0.1% TFA). The product was subjected to gel filtration with Sephadex G-10 and then purified by RP-HPLC. Mass data of these peptides are described in Supporting Information.

**Folding of  $\delta$ C1b Domains.** Purified peptides were dissolved in 50 mM Tris·HCl (pH 7.4) with 5 mM DTT, incubated for 15 min at 30 °C, and then stored at –20 °C with 20% glycerol. The peptide solution was dialyzed against 50 mM Tris·HCl (pH 7.4) containing 150 mM NaCl, 1 mM DTT, and 0.1 mM ZnCl<sub>2</sub> using a Slide-A-Lyzer Dialysis Cassette 2000 MWCO (Thermo Scientific).

**[<sup>3</sup>H]PDBu Binding Assay.** [<sup>3</sup>H]PDBu binding to the  $\delta$ C1b domains was measured using the poly(ethylene glycol) precipitation assay as described previously (18, 19) with minor modifications. To determine the dissociation constants ( $K_d$ ) and numbers of binding sites ( $B_{max}$ ) for the dansyl-labeled  $\delta$ C1b domains, saturation curves with increasing concentrations of [<sup>3</sup>H]PDBu were obtained in triplicate. 250  $\mu$ L of the assay mixture contained 50 mM Tris·HCl (pH 7.4), 1 mM ethylenediaminetetraacetic acid (EGTA), 0.1 mg/mL phosphatidylserine, 5 mg/mL bovine immunoglobulin G, variable concentrations of [<sup>3</sup>H]PDBu, and, for those tubes used to determine nonspecific binding, an excess of nonradioactive PDBu. After addition of peptides stored in 0.015% Triton X-100, binding was carried out at 18 °C for 10 min. Samples were incubated on ice for 10 min. 200  $\mu$ L of 35% poly(ethylene glycol) in 50 mM Tris·HCl (pH 7.4) was added, and the samples were incubated on ice for an additional 10 min. The tubes were centrifuged at 4 °C (12 200 rpm, 15 min), and a 100  $\mu$ L aliquot of each supernatant was then transferred to a scintillation vial for determination of the amount of the free [<sup>3</sup>H]PDBu. After the remaining supernatant was aspirated off, the bottom of each centrifuge tube was cut off just above the pellet and transferred to a scintillation vial for the determination of the amount of the total bound [<sup>3</sup>H]PDBu. Dissociation constants ( $K_d$ ) were calculated by Scatchard analysis.

**CD Measurement.** CD spectra were recorded on a Jasco J-720 spectropolarimeter at 25 °C. The measurements were

performed at 0.1 nm spectral resolution using a 0.5 cm path length quartz cuvette. Each spectrum represents the average of 40 scans, and the scan rate was 100 nm/min. Measurements were performed in a Tris·HCl (pH 7.4) buffer containing 1 mM DTT and 150 mM NaCl.

**Fluorescence Measurement.** Ligand titration was performed in 1 mL of dialysis buffer containing 0.5  $\mu$ M dialyzed dansyl-labeled  $\delta$ C1b domain and 5  $\mu$ g/mL phosphatidylserine at 25 °C. After each addition of ligands, the mixture was incubated at the same temperature for 10 min. Fluorescent emission spectra ( $\lambda_{ex}$  = 330 nm; slit width: 20 nm for excitation, 40 nm for emission) were obtained throughout the addition of ligands. For experiments using 96-cell plates, Dansyl-labeled  $\delta$ C1b domain solution (dialysis buffer containing 0.5  $\mu$ M dialyzed peptides and 5  $\mu$ g/mL phosphatidylserine) was prepared and incubated for 10 min at room temperature. Fluorescence of dansyl-labeled  $\delta$ C1b domain was measured using an excitation filter of 355 nm (half-width: 40 nm) and an emission filter of 460 nm (half-width: 25 nm), respectively.

**Molecular Modeling.** Molecular modeling was performed using Sybyl 7.1 (Tripos Inc., St. Louis, MO). Predictive models of dansyl-labeled  $\delta$ C1b domain analogues were built by substitution of Lys(Dns-Gly) for residues Tyr238, Ser240, or Thr242 that were contained in the crystal structure of  $\delta$ C1b domain (PDB 1PTR) (20). Energy-minimization was performed on the Lys(Dns-Gly) moiety using the Tripos force field and Gasteiger-Huckel charge parameters.

## RESULTS AND DISCUSSION

**Design of Fluorescent-Labeled PKC $\delta$  C1b Domains.** Residues 221–281 of PKC $\delta$  forming the C1b domain represent the starting sequence we used for modification. To identify the optimal amino acid position for fluorescent labeling, Tyr238, Ser240, and Thr242 were selected for evaluation. Our choice was based on the following rationale: First, these residues are located at the edge of the binding pocket of the C1b domain as shown by the structure of  $\delta$ C1b-phorbol ester complex (20). Second, site-directed mutagenesis had shown that Ser240 was not necessary for the phorbol ester binding and that the  $\delta$ C1b domain mutants T242G, T242S, and T242 V had only minimal effects on the binding affinity of PDBu (2.1-, 1.1-, and 3.2-fold, respectively) (21). Third, replacement of Tyr by Gly in position 238 reduced binding affinity of [<sup>3</sup>H]PDBu by 60-fold, but maintained nanomolar affinity ( $K_d$  = 48  $\pm$  3.0 nM), which might be sufficient for the detection of PKC ligands (21). A chemically modified lysine was utilized for fluorescent labeling. For this study, a dansyl group was adopted because of its small molecular size and larger Stokes shift compared to NBD (22). Since the flexibility of the dansyl moiety might contribute to its sensitivity to ligand binding to the  $\delta$ C1b domain, glycine was incorporated between the  $\epsilon$ -amino group of lysine and the dansyl moiety as a linker to construct Lys(Dns-Gly) (Supporting Information Scheme S1). Three  $\delta$ C1b domain analogues, in which Lys(Dns-Gly) was substituted for Tyr238, Ser240, or Thr242, were designed and designated as Y238K(DnsG), S240K(DnsG), and T242K(DnsG), respectively. Predictive structural models of the dansyl-labeled  $\delta$ C1b domains were constructed based on the crystal structure of the  $\delta$ C1b domain (PDB entry 1PTR) utilizing Sybyl 7.1 (Figure 1). The models showed that the dansyl moieties of S240K(DnsG) and T242K(DnsG) are located outside the binding pocket, whereas the dansyl moiety of Y238K(DnsG) was located inside.

**Synthesis of Dansyl-Labeled  $\delta$ C1b Domain Analogues.** Fmoc-protected Lys(Dns-Gly) (4) was synthesized as described in Supporting Information Scheme S1.  $\delta$ C1b domain analogues were synthesized based on the standard Fmoc solid-phase peptide synthesis (SPPS) (23). For an efficient synthesis of

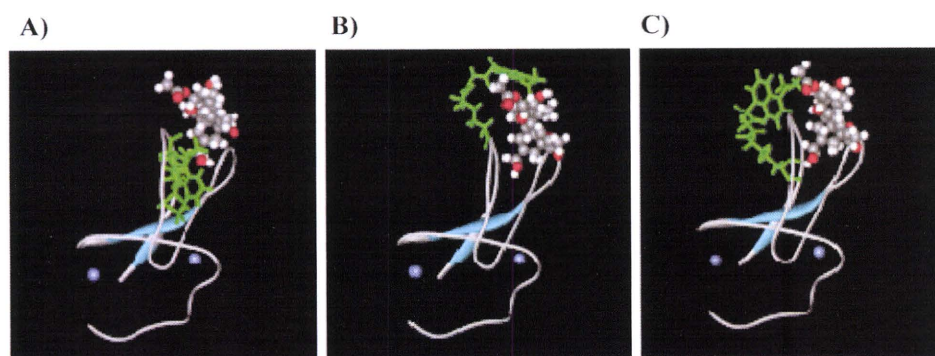


**Figure 1.** Structural models of dansyl-labeled  $\delta$ C1b analogues. (A) Y238K(DnsG), (B) S240K(DnsG), and (C) T242K(DnsG). Space-filling models indicate phorbol esters and zinc atoms.

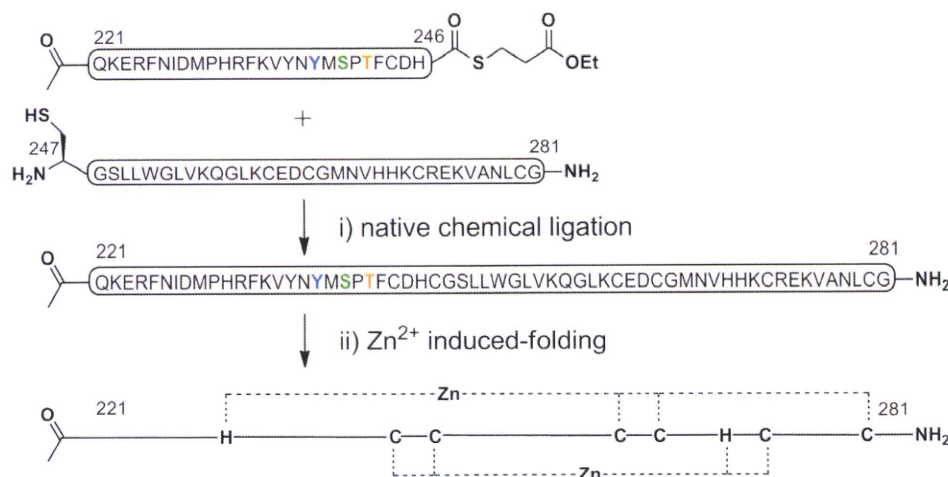


**Figure 2.** Schematic representation of construction of dansyl-labeled  $\delta$ C1b. (i) 100 mM phosphate buffer (pH 8.5), 6 M  $\text{Gn}\cdot\text{HCl}$ , 2 mM EDTA, TCEP $\cdot\text{HCl}$ , thiophenol,  $\text{N}_2$ , 37 °C; (ii) 50 mM Tris $\cdot\text{HCl}$  (pH 7.4), 150 mM NaCl, 1 mM DTT, 0.1 mM  $\text{ZnCl}_2$ , 4 °C.

dansyl-labeled  $\delta$ C1b domain analogues, a native chemical ligation (NCL) method was adopted (18, 24). Three N-terminal peptide fragments (dansyl-labeled  $\delta$ C1b(221–246)) and a common C-terminal peptide fragment ( $\delta$ C1b(247–281)) were separately synthesized. A purified  $\delta$ C1b(247–281) and three dansyl-labeled  $\delta$ C1b(221–246) fragments were condensed by an NCL method (Figure 2). The ligation reaction was performed with 0.8 mM of each peptide fragment in 100 mM phosphate buffer (pH 8.5) containing 6 M  $\text{Gn}\cdot\text{HCl}$ , 2 mM EDTA, and 3% thiophenol at 37 °C. The progress of the ligation reaction was monitored by HPLC (Supporting Information). The condensed  $\delta$ C1b domains were identified by ESI-TOF-mass spectra (Supporting Information Table S1). The purified peptides were lyophilized and obtained as powders. Total yields of NCL were 38% for Y238K(DnsG), 48% for S240K(DnsG), and 41% for T242K(DnsG). Folding of the synthetic  $\delta$ C1b domain was performed by dialysis against  $\text{Zn}^{2+}$  containing buffer (50 mM Tris $\cdot\text{HCl}$  (pH 7.4), 150 mM NaCl, 1 mM DTT, 0.1 mM  $\text{ZnCl}_2$ ) at 4 °C.

**Characterization of Synthetic  $\delta$ C1b Analogues.** The apparent [ $^3\text{H}$ ]PDBu binding affinity of the dansyl-labeled  $\delta$ C1b domains was evaluated by the method described previously (18, 19). S240K(DnsG) and T242K(DnsG) showed  $K_d$  values comparable to that of the wild type. However,  $B_{\text{max}}$  values were 6% for S240K(DnsG) and 11% for T242K(DnsG) compared to the wild type (Table 1). The results indicate that dansyl-labeling might partly impair the efficiency of correct folding of the synthetic  $\delta$ C1b domain. Y238K(DnsG) did not possess significant binding affinity for PDBu, consistent with the predictions from the modeling. We conclude that the dansyl-labeled  $\delta$ C1b domains maintain potent binding activity and correct folding, at least for an appreciable proportion of the

**Table 1. Binding Activity of the Synthetic  $\delta$ C1b Analogues to [ $^3\text{H}$ ]PDBu**

peptides	$K_d$ (nM) <sup>a</sup>	$B_{\text{max}}$ (pmol/mg) <sup>b</sup>
wild type	0.34 ± 0.08	38000
Y238K(DnsG)	n.d. <sup>c</sup>	11
S240K(DnsG)	0.18 ± 0.05	2100
T242K(DnsG)	0.35 ± 0.04	3700

<sup>a</sup> Dissociation constant for the synthetic  $\delta$ C1b binding to [ $^3\text{H}$ ]PDBu. Mean ± SEM. <sup>b</sup> Numbers of binding sites. <sup>c</sup> Not determined.

product, in those cases in which the dansyl group is located outside the binding pocket.

To estimate the influence of dansyl-labeling on folding of  $\delta$ C1b domain, circular dichroism (CD) spectroscopy of S240K(DnsG) and T242K(DnsG) was performed for comparison before and after dialysis (Figure 3). Since the CD spectrum of the synthetic  $\delta$ C1b(231–281) is similar to that of the recombinant  $\delta$ C1b domain (18), Y238K(DnsG)- $\delta$ C1b(231–281) was used to evaluate the effects of dansyl-labeling on folding of Y238K(DnsG) (Supporting Information Figure S3). The addition of  $\text{ZnCl}_2$  did not cause a significant change of CD spectra of Y238K(DnsG)- $\delta$ C1b(231–281). Thus, the introduction of a dansyl group into Tyr238 might interfere correct folding. The CD spectra of both of the dansyl-labeled  $\delta$ C1b domains before dialysis showed broad minima around 205 nm, suggesting random coil structures (25). CD spectra of the dialyzed dansyl-labeled  $\delta$ C1b domains exhibited decreases of negative cotton effects around 205 nm, which were similar to those of recombinant and synthetic  $\delta$ C1b domains (18, 25).

The apparent [ $^3\text{H}$ ]PDBu binding affinities and CD spectra of the dansyl-labeled  $\delta$ C1b domains, S240K(DnsG) and

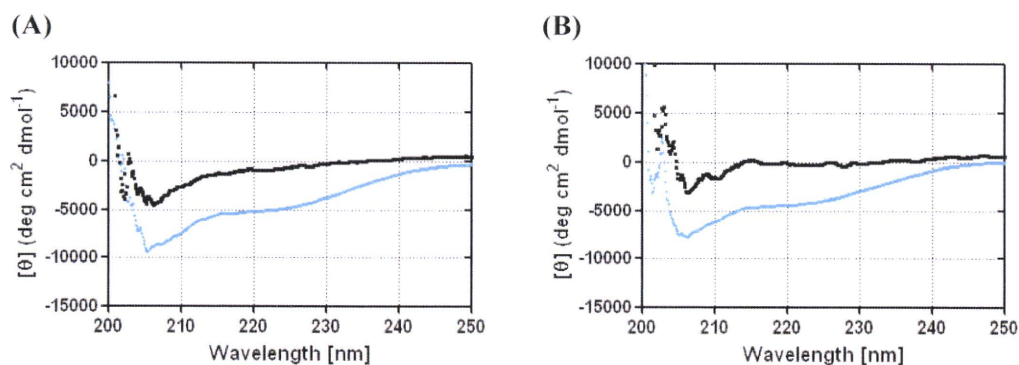


**Figure 3.** Changes of CD spectra of dansyl-labeled  $\delta$ C1b analogues, S240K(DnsG) (A) and T242K(DnsG) (B). Blue and black plots show profiles before and after dialysis against  $\text{Zn}^{2+}$  containing buffer, respectively.

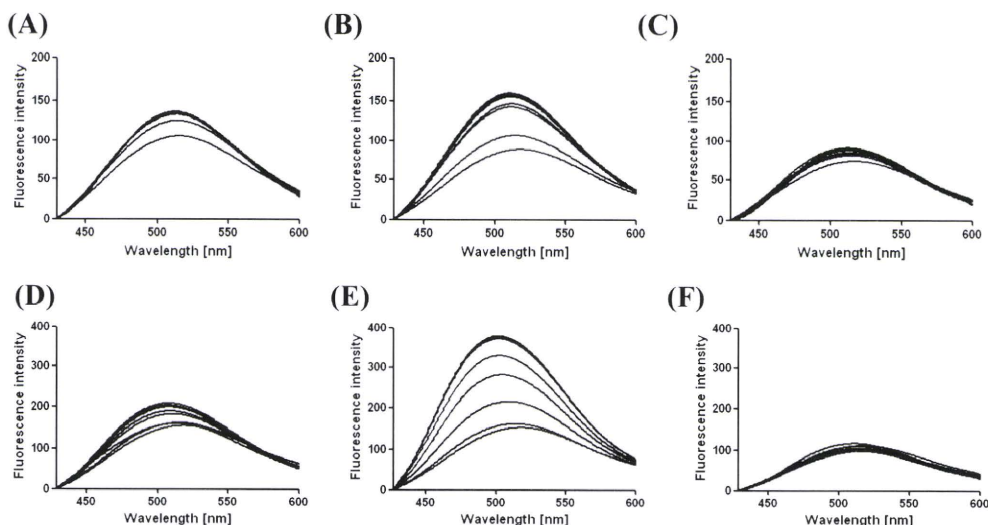


**Figure 4.** Fluorescent spectra obtained by ligand titration experiments for dansyl-labeled  $\delta$ C1b analogues. Panels A–C show titrations of PDBu, PMA, and PDA against S240K(DnsG), respectively. Panels D–F show titrations of PDBu, PMA, and PDA against T242K(DnsG), respectively. Dansyl-labeled  $\delta$ C1b analogue,  $0.5 \mu\text{M}$ ; buffer, 50 mM Tris·HCl (pH 7.4), 150 mM NaCl, 1 mM DTT, 0.1 mM  $\text{ZnCl}_2$ ,  $5 \mu\text{g/mL}$  phosphatidylserine; ligand, 0.02, 0.06, 0.1, 0.14, 0.18, 0.22, 0.26, 0.3 equiv,  $\lambda_{\text{ex}} = 330 \text{ nm}$ .

T242K(DnsG), demonstrated that insertion of dansyl groups at Ser 240 and at Thr 242 maintained correct folding and strong ligand binding affinity comparable to that of the wild type, although involving reduction of the stability of the domains.

**Titration of Ligands to Fluorescent-Labeled  $\delta$ C1b Domain Analogues.** To evaluate the fluorescent properties of dansyl-labeled  $\delta$ C1b domain, fluorescent emission spectra were measured during ligand titration. As test ligands, the phorbol esters PDBu ( $K_i = 0.72 \pm 0.06 \text{ nM}$ ), phorbol 12-myristate 13-acetate (PMA) ( $K_i = 0.14 \pm 0.04 \text{ nM}$ ), and phorbol 12,13-diacetate (PDA) ( $K_i = 68.9 \pm 5.9 \text{ nM}$ ), were employed. Values of  $K_i$  were determined by competitive binding assays using [ $^3\text{H}$ ]PDBu (Supporting Information). Fluorescent titration experiments showed that the spectra of the dansyl-labeled  $\delta$ C1b domain analogues changed according to the ligand concentration. S240K(DnsG) showed 1.3-, 1.8-, and 1.2-fold increases in fluorescent intensity and blue shifts in the emission maxima upon additions of PDBu, PMA, and PDA, respectively (Figures 4A–C). T242K(DnsG) showed 1.3-, 2.6-, and 1.1-fold increases in fluorescent intensity and blue shifts in the emission maxima upon additions of PDBu, PMA, and PDA, respectively (Figures 4D–F). The rank order of increases in fluorescent intensity upon addition of the above ligands to S240K(DnsG) and T242K(DnsG) thus corresponded to that of their  $K_i$  values.

Since dansyl-Gly showed stronger fluorescent intensity in a hydrophobic environment than in a hydrophilic environment

(Supporting Information Figure S1), the increases in fluorescence intensity upon ligand titration of S240K(DnsG) and T242K(DnsG) suggested that the environment surrounding the dansyl moiety was changed to become more hydrophobic upon ligand binding (26–28). As predicted in the modeling study, the dansyl group was not located in the binding pocket, preventing binding. Even after ligand binding, the dansyl group will still be located outside the binding pocket. Thus, the binding of ligands to the binding pocket must make the environment surrounding the dansyl moiety more hydrophobic, possibly due to interactions between dansyl and the long alkyl chains of the ligands. In addition, T242K(DnsG) showed stronger fluorescence intensity than did S240K(DnsG). This phenomenon corresponds to their relative  $B_{\text{max}}$  values observed in the [ $^3\text{H}$ ]PDBu binding assay (Figures 1B, C, Table 1). A reason could be the hydrogen bonding network at the binding site of phorbol ester on the  $\delta$ C1b domain. The C20 hydroxy group of the phorbol ester accepts a hydrogen bond from the main-chain NH of T242 (20). Thus, the stronger fluorescent intensity of T242K(DnsG) could be due to a closer distance to the bound ligand. Furthermore, saturation of the increase in fluorescent intensity was observed when the ligand concentration reached  $0.05\text{--}0.1 \mu\text{M}$  (10–20% of the peptide concentration) (Figure 5). This result is consistent with the  $B_{\text{max}}$  values of dansyl-labeled  $\delta$ C1b: 6–11% of the wild type. The  $K_d$  values based on titration of ligands to the dansyl-labeled  $\delta$ C1b domains were evaluated (Table 2). As a control experiment, S240K(DnsG) dialyzed without  $\text{Zn}^{2+}$  did not



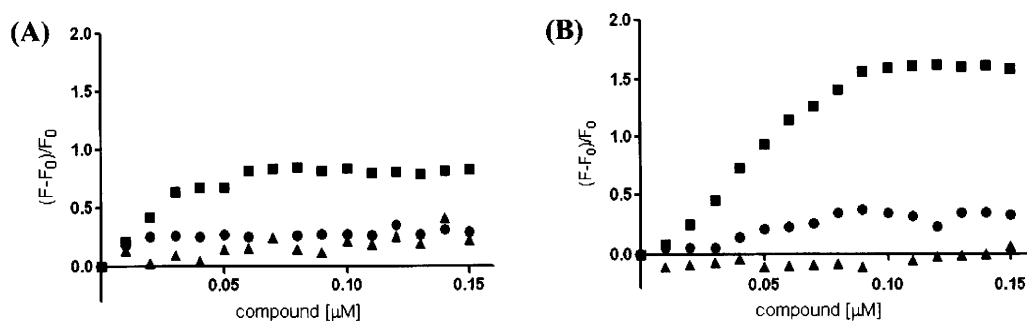
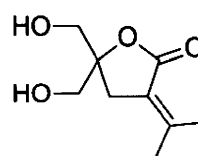
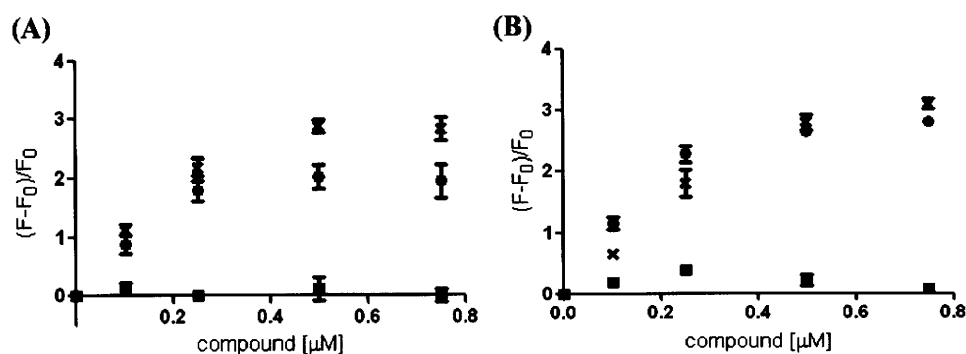


**Figure 5.** Plots of change of fluorescence intensity from titration experiments using S240K(DnsG) (A) and T242K(DnsG) (B). Dansyl-labeled  $\delta$ C1b analogue, 0.5  $\mu$ M; square, PMA; round, PDBu; triangle, PDA.



DAG-lactone derivative

**Figure 6.** Plots of change of fluorescence intensity from 96-well plates-based titration experiments of S240K(DnsG) (A) and T242K(DnsG) (B). cross, PMA; circle, PDBu; square, DAG-lactone derivative.

**Table 2.**  $K_d$  Values of the Fluorescent-Labeled  $\delta$ C1b Domain Analogues Based on Titration of Ligands

compound	S240K(DnsG) $K_d$ (nM) <sup>a</sup>	T242K(DnsG) $K_d$ (nM) <sup>a</sup>
PMA	20.6	121.6
PDBu	5.83	110
PDA	Not convergent	Not fitting

<sup>a</sup> Dissociation constant for the fluorescent-labeled  $\delta$ C1b domain analogues to each compound was calculated.

show any significant increase in fluorescent intensity upon the addition of PDBu (Supporting Information Figure S2), suggesting that correct folding involving zinc-finger formation is critical for ligand binding. The detection limit might be the level of the fluorescent intensity of PDA. The results of titration experiments indicate that, upon ligand binding to correctly folded C1b domains, the site surrounding the ligand binding pocket becomes more hydrophobic. Even if some uncertainty remains about the relative contributions of the mechanisms leading to this change in hydrophobicity, the core finding is that ligand binding was detected by an increase in fluorescent intensity, which corresponds to binding affinity. The binding activity of ligands can be possibly evaluated by increases in fluorescent intensity upon the consideration of LogP values.

S240K(DnsG) and T242K(DnsG) were employed in fluorescent experiments utilizing 96-well plates for initial assessment of their suitability to high-throughput screening. Plots of changes of fluorescent intensity against the ligand concentration showed dose-dependent curves similar to those in titration experiments (Figure 6). The results indicate that the present fluorescent-

responsive C1b domains can be used for screening of novel PKC pharmacophores.

## CONCLUSIONS

In this study, three kinds of dansyl-labeled  $\delta$ C1b domains, Y238K(DnsG), S240K(DnsG), and T242K(DnsG), were synthetically constructed in an efficient way by utilizing Fmoc-SPPS and an NCL method. The results of CD measurements and [<sup>3</sup>H]PDBu binding assays indicated that the position of dansyl-labeling was critical for maintenance of native functions including proper folding. The ligand titration of dansyl-labeled  $\delta$ C1b showed that the change of fluorescent spectra corresponded to the  $K_i$  values of the ligands. Furthermore, S240K(DnsG) and T242K(DnsG) were utilized for measurements using a 96-well plate-based format, indicating that evaluation of ligand binding could be performed in a high-throughput fashion. The present fluorescent-responsive domains were successfully utilized in vitro. However, through optimization of the stability of the fluorescent-labeled  $\delta$ C1b domain, these domains might also be adapted for cell-based assays as efficient DAG sensors.

## ACKNOWLEDGMENT

The authors thank Professor Kazunari Akiyoshi (Graduate School of Engineering, Kyoto University) for assistance in the CD experiments. This study was supported in part by the Naito Foundation for Science (to W. N.) and in part by the Intramural Research Program of the NIH, Center for Cancer Research, National Cancer Institute. N. O. is supported by the Japan Society for Promotion of Science.

**Supporting Information Available:** Detailed materials and methods. This material is available free of charge via the Internet at <http://pubs.acs.org>.

## LITERATURE CITED

- (1) Nishizuka, Y. (1992) Intracellular signaling by hydrolysis of phospholipids and activation of protein kinase C. *Science* 258, 607–614.
- (2) Newton, A. C. (1995) Protein kinase C: structure, function, and regulation. *J. Biol. Chem.* 270, 28495–28498.
- (3) Watanabe, T., Ono, Y., Taniyama, Y., Hazama, K., Igarashi, K., Ogita, K., Kikkawa, U., and Nishizuka, Y. (1992) Cell division arrest induced by phorbol ester in CHO cells overexpressing protein kinase C-delta subspecies. *Proc. Natl. Acad. Sci. U.S.A.* 89, 10159–10163.
- (4) Mischak, H., Pierce, J. H., Goodnight, J., Kazanietz, M. G., Blumberg, P. M., and Mushinski, J. F. (1993) Phorbol ester-induced myeloid differentiation is mediated by protein kinase C-alpha and -delta and not by protein kinase C-beta II, -epsilon, -zeta, and -eta. *J. Biol. Chem.* 268, 20110–20115.
- (5) Li, C., Wernig, E., Leitges, M., Hu, Y., and Xu, Q. (2003) Mechanical stress-activated PKCdelta regulates smooth muscle cell migration. *FASEB J.* 17, 2106–2108.
- (6) Ghayur, T., Hugunin, M., Talanian, R. V., Ratnofsky, S., Quinlan, C., Emoto, Y., Pandey, P., Datta, R., Huang, Y., Kharbanda, S., Allen, H., Kamen, R., Wong, W., and Kufe, D. (1996) Proteolytic activation of protein kinase C delta by an ICE/CED 3-like protease induces characteristics of apoptosis. *J. Exp. Med.* 184, 2399–2404.
- (7) Humphries, M. J., Limesand, K. H., Schneider, J. C., Nakayama, K. I., Anderson, S. M., and Reyland, M. E. (2006) Suppression of apoptosis in the protein kinase Cdelta null mouse in vivo. *J. Biol. Chem.* 281, 9728–9737.
- (8) Alkon, D. L., Sun, M. K., and Nelson, T. J. (2007) PKC signaling deficits: a mechanistic hypothesis for the origins of Alzheimer's disease. *Trends Pharmacol. Sci.* 28, 51–60.
- (9) Churchill, E., Budas, G., Vallentin, A., Koyanagi, T., and Mochly-Rosen, D. (2008) PKC isozymes in chronic cardiac disease: possible therapeutic targets? *Annu. Rev. Pharmacol. Toxicol.* 48, 569–599.
- (10) O'Brian, C. A., Ward, N. E., Stewart, J. R., Chu, F., Mackay, H. J., and Twelves, C. (2001) Prospects for targeting protein kinase C isozymes in the therapy of drug-resistant cancer—an evolving story. *Cancer Metastasis Rev.* 20, 95–100.
- (11) Tamamura, H., Sigano, D. M., Lewin, N. E., Blumberg, P. M., and Marquez, V. E. (2004) Conformationally constrained analogues of diacylglycerol. 20. The search for an elusive binding site on protein kinase C through relocation of the carbonyl pharmacophore along the sn-1 side chain of 1,2-diacylglycerol lactones. *J. Med. Chem.* 47, 644–655.
- (12) Tamamura, H., Sigano, D. M., Lewin, N. E., Peach, M. L., Nicklaus, M. C., Blumberg, P. M., and Marquez, V. E. (2004) Conformationally constrained analogues of diacylglycerol (DAG). 23. Hydrophobic ligand-protein interactions versus ligand-lipid interactions of DAG-lactones with protein kinase C (PK-C). *J. Med. Chem.* 47, 4858–4864.
- (13) Marquez, V. E., and Blumberg, P. M. (2003) Synthetic diacylglycerols (DAG) and DAG-lactones as activators of protein kinase C (PK-C). *Acc. Chem. Res.* 36, 434–443.
- (14) Morii, T., Sugimoto, K., Makino, K., Otsuka, M., Imoto, K., and Mori, Y. (2002) A new fluorescent biosensor for inositol trisphosphate. *J. Am. Chem. Soc.* 7, 1138–1139.
- (15) Venkatraman, P., Nguyen, T. T., Sainlos, M., Bilsel, O., Chitta, S., Imperiali, B., and Stern, L. J. (2007) Fluorogenic probes for monitoring peptide binding to class II MHC proteins in living cells. *Nat. Chem. Biol.* 3, 201–202.
- (16) Joshi, B. P., and Lee, K. H. (2008) Synthesis of highly selective fluorescent peptide probes for metal ions: tuning selective metal monitoring with secondary structure. *Bioorg. Med. Chem.* 16, 8501–8509.
- (17) Simard, J. R., Grütter, C., Pawar, V., Aust, B., Wolf, A., Rabiller, M., Wulfert, S., Robubi, A., Klüter, S., Ottmann, C., and Rauh, D. (2009) High-throughput screening to identify inhibitors which stabilize inactive kinase conformations in p38 $\alpha$ . *J. Am. Chem. Soc.* 131, 18478–18488.
- (18) Ohashi, N., Nomura, W., Kato, M., Narumi, T., Lewin, N. E., Blumberg, P. M., and Tamamura, H. (2009) Synthesis of protein kinase C $\delta$  C1b domain by native chemical ligation methodology and characterization of its folding and ligand binding. *J. Pept. Sci.* 10, 642–646.
- (19) Kazanietz, M. G., Areces, L. B., Bahador, A., Mischak, H., Goodnight, J., Mushinski, J. F., and Blumberg, P. M. (1993) Characterization of ligand and substrate specificity for the calcium-dependent and calcium-independent protein kinase C isozymes. *Mol. Pharmacol.* 44, 298–307.
- (20) Zhang, G., Kazanietz, M. G., Blumberg, P. M., and Hurley, J. H. (1995) Crystal structure of the cys2 activator-binding domain of protein kinase C delta in complex with phorbol ester. *Cell* 81, 917–924.
- (21) Kazanietz, M. G., Wang, S., Milne, G. W., Lewin, N. E., Liu, H. L., and Blumberg, P. M. (1995) Residues in the second cysteine-rich region of protein kinase C delta relevant to phorbol ester binding as revealed by site-directed mutagenesis. *J. Biol. Chem.* 270, 21852–21859.
- (22) Soini, E., and Hemmila, I. (1979) Fluoroimmunoassay: present status and key problems. *Clin. Chem.* 25, 353–361.
- (23) Irie, K., Oie, K., Nakahara, A., Yanai, Y., Ohigashi, H., Wender, P. A., Fukuda, H., Konishi, H., and Kikkawa, U. (1998) Molecular basis for protein kinase C isozyme-selective binding: the synthesis, folding, and phorbol ester binding of the cysteine-rich domains of all protein kinase C isozymes. *J. Am. Chem. Soc.* 120, 9159–9167.
- (24) Dawson, P. E., Churchill, M. J., Ghadiri, M. R., and Kent, S. B. H. (1997) Chemical protein synthesis by solid phase ligation of unprotected peptide segments. *J. Am. Chem. Soc.* 119, 4325–4329.
- (25) Zimenkov, Y., Dublin, S. N., Ni, R., Tu, R. S., Breedveld, V., Apkarian, R. P., and Conticell, V. P. (2006) Rational design of a reversible pH-responsive switch for peptide self-assembly. *J. Am. Chem. Soc.* 128, 6770–6771.
- (26) Ikeda, H., Nakamura, M., Ise, N., Oguma, N., Nakamura, A., Ikeda, T., Toda, F., and Ueno, A. (1996) Fluorescent cyclodextrins for molecule sensing: fluorescent properties, NMR characterization, and inclusion phenomena of n-dansylleucine-modified cyclodextrins. *J. Am. Chem. Soc.* 118, 10980–10988.
- (27) Ikunaga, T., Ikeda, H., and Ueno, A. (1999) The effects of avidin on inclusion phenomena and fluorescent properties of biotin-appended dansyl-modified  $\beta$ -cyclodextrin. *Chem.—Eur. J.* 5, 2698–2704.
- (28) Matsumura, S., Sakamoto, S., Ueno, A., and Mihara, H. (2000) Construction of  $\alpha$ -helix peptides with  $\beta$ -cyclodextrin and dansyl units and their conformational and molecular sensing properties. *Chem.—Eur. J.* 6, 1781–1788.

BC100414A

## Bivalent Ligands of CXCR4 with Rigid Linkers for Elucidation of the Dimerization State in Cells

Tomohiro Tanaka, Wataru Nomura,\* Tetsuo Narumi, Akemi Masuda, and Hirokazu Tamamura\*

Department of Medicinal Chemistry, Institute of Biomaterials and Bioengineering, Tokyo Medical and Dental University, 2-3-10 Kandasurugadai, Chiyoda-ku, Tokyo 101-0062, Japan

Received August 18, 2010; E-mail: nomura.mr@tmd.ac.jp; tamamura.mr@tmd.ac.jp

**Abstract:** To date, challenges in the design of bivalent ligands for G protein-coupled receptors (GPCRs) have revealed difficulties stemming from lack of knowledge of the state of oligomerization of the GPCR. The synthetic bivalent ligands with rigid linkers that are presented here can predict the dimer form of CXCR4 and be applied to molecular probes in cancerous cells. This “molecular ruler” approach would be useful in elucidating the details of CXCR4 oligomer formation.

The chemokine receptor CXCR4 is a membrane protein belonging to the family of G protein-coupled receptors (GPCRs). In current drugs, ~60% of drug target molecules are located at the cell surface, and half of them are GPCRs.<sup>1</sup> Recent studies have indicated a pivotal role for homo- and heterooligomerization of CXCR4 in cancer metastasis, and the significance of oligomeric forms of GPCR has been gaining acceptance.<sup>2</sup> However, the functional implications proposed for these oligomers, which include signal transduction and internalization, are poorly understood and require additional studies.<sup>3</sup> Efforts to understand those correlations have used photochemical analyses such as bioluminescence resonance energy transfer (BRET) analysis,<sup>3,4</sup> but the elucidation of the native state of CXCR4 in living cells is complicated by conformational or functional changes resulting from mutations. Estimates of the precise distance between ligand binding sites in the dimer form would permit the development of bivalent ligands of CXCR4 having improved binding affinity and specificity.<sup>5</sup> In spite of the enormous effort devoted to the design of bivalent ligands, rational design of such linkers has been difficult because of the lack of knowledge concerning the dimeric form of GPCRs. Therefore, there is an increasing demand for a novel strategy for the analysis of the precise distance between ligand binding sites.<sup>6</sup>

In this study, we designed and synthesized novel CXCR4 bivalent ligands consisting of two molecules of an FC131<sup>7</sup> analogue, [*cyclo*(D-Tyr-Arg-Arg-Nal-D-Cys-)] [Nal = L-3-(2-naphthyl)alanine, **1a**], connected by a poly(L-proline) or a PEGylated poly(L-proline) linker. Poly(L-prolines) have been utilized as rigid linkers between the two functional units, which require a predetermined separation for activity.<sup>8</sup> Linkers consisting of poly(L-prolines) were expected to maintain constant distances of 2–8 nm between the ligands. Our bivalent ligands with linkers of various lengths were used to determine the distance between two binding sites of ligands consisting of CXCR4 dimers. Acetamide-capped FC131 (**1b**), in which Gly is replaced by D-Cys and the thiol group of Cys is capped with an acetamide group, was synthesized as a monomer unit of the ligand (Figure 1). Although this substitution caused a 2-fold decrease in binding to CXCR4, the binding affinity was still adequate for analyses. Poly(L-proline) helices are known to maintain a length of 0.9 nm per turn.<sup>9</sup> In this study, polyproline- and

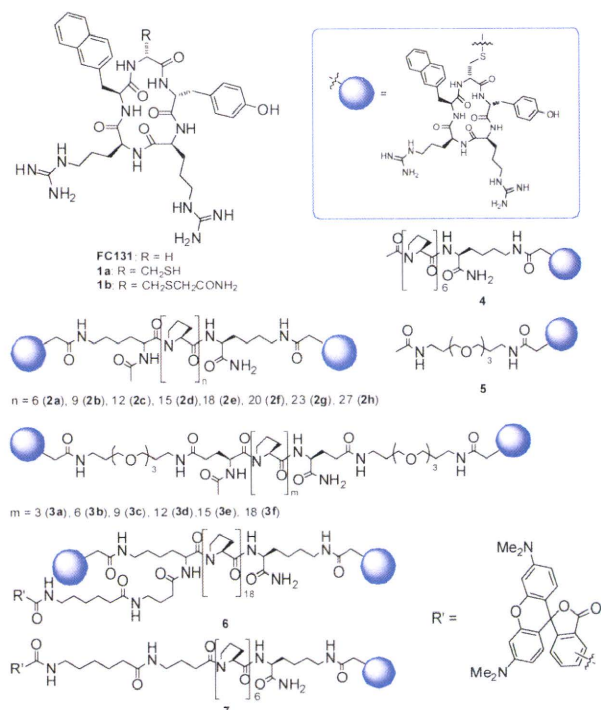


**Figure 1.** Design of bivalent ligands against chemokine receptor CXCR4. As CXCR4 binding moieties, D-Cys FC131 (R = CH<sub>2</sub>SH, **1a**) and acetamide-capped FC131 (R = CH<sub>2</sub>SCH<sub>2</sub>CONH<sub>2</sub>, **1b**) were prepared. Poly(L-proline) (**2a–h**) and PEG-conjugated poly(L-proline) (**3a–f**) with CXCR4 binding moieties on both ends were synthesized. As monomer binding ligands with linkers, Ac<sub>6</sub>pro FC131 (**4**) and AcPEG FC131 (**5**) were synthesized. Tetramethylrhodamine (TAMRA)-labeled **2e** (**6**) and **4** (**7**) were prepared for the imaging experiments.

PEGylated polyproline-type linkers with lengths of 2–8 nm were synthesized.<sup>10</sup> The synthetic linkers and their conjugated bivalent ligands were characterized by high-resolution mass spectrometry (HRMS) (Tables S3 and S5 in the Supporting Information), and their CD spectra clearly showed the presence of a type-II polyproline helix (Figure S3 in the Supporting Information). As monomer controls, FC131 analogues **4** and **5** with hexaproline and poly(ethylene glycol) (PEG) linkers, respectively, that were acetylated at the other end were also prepared.

The binding affinities of the synthetic ligands were evaluated in a competitive binding assay against [<sup>125</sup>I]-SDF-1α, as reported previously.<sup>7d</sup> The binding assay showed that the binding affinity of our bivalent ligands is clearly dependent on the linker length. Ligands of the poly(L-proline) type with the highest affinities were **2e** and **2f**. Among the PEGylated poly(L-proline)-type ligands, **3c** and **3d** showed the highest affinity. The linker-optimized bivalent ligands, **2f** and **3d**, showed 7.3- and 21-fold increases in binding affinity relative to **4** and **5**, respectively (Table 1). These results

**Table 1.** Summary of Binding Affinities of Synthetic Bivalent and Monovalent Ligands Analyzed by [<sup>125</sup>I]-SDF-1 $\alpha$  Competition Assay

compd	K <sub>i</sub> (nM) <sup>a</sup>	linker length (nm)	compd	K <sub>i</sub> (nM) <sup>a</sup>	linker length (nm)
FC131	31.5	—	<b>3a</b>	87.2	3.8
<b>1b</b>	53.4	—	<b>3b</b>	45.6	4.7
<b>2a</b>	51.2	1.8	<b>3c</b>	17.8	5.6
<b>2b</b>	45.4	2.7	<b>3d</b>	13.9	6.5
<b>2c</b>	64.4	3.6	<b>3e</b>	49.3	7.4
<b>2d</b>	59.5	4.5	<b>3f</b>	83.3	8.3
<b>2e</b>	13.2	5.4	<b>4</b>	72	—
<b>2f</b>	9.9	6	<b>5</b>	294	—
<b>2g</b>	22.5	6.9	<b>7</b>	119	—
<b>2h</b>	45.8	8.1			

<sup>a</sup> K<sub>i</sub> values are the concentrations corresponding to 50% inhibition of [<sup>125</sup>I]-SDF-1 $\alpha$  binding to Jurkat cells.

indicate successful bivalent binding of the ligands, which has been known to be responsible for an increase in binding affinity.<sup>5a</sup> It should be noted that the maximum increase in binding affinity was observed for ligands of the two linker types having similar lengths (5.5–6.5 nm). In the dimer state of CXCR4, there are several forms of assembly (head-to-head, tail-to-tail, and head-to-tail).<sup>5a</sup> These forms have different distances between the binding sites of the ligands. Molecular modeling studies of FC131 with CXCR4 suggested that amino acids in transmembrane (TM) 7 are important for FC131 binding.<sup>11</sup> Through the use of the rhodopsin structure, it was revealed that in the TM 4 and 5 assembly form, the linear distance between ligand binding sites is 5.3 nm. In the other forms of possible assembly, the linear distances were determined to be 3.5 and 3.9 nm for TM 1 and 2 assembly and the combination of TM 1–4 and TM 2–5 assembly, respectively (Figure S4). The changes in binding affinity were relatively moderate, and although the existence of different assembly forms is possible, a majority of the population should be in the TM 4 and 5 assembly form.

From the increased binding affinity of linker-optimized bivalent ligands, a hypothesis was derived that such ligands could be applied as probes specific to CXCR4 on the cell surface because the receptors are overexpressed in several kinds of malignant cells<sup>12</sup> and that the dimer formation of the receptor should depend on the expression level. Accordingly, compound **2e**, which showed high binding affinity, was chosen for labeling with tetramethylrhodamine (TAMRA) and applied to the imaging of CXCR4. The TAMRA moiety was conjugated to an N-terminal of the proline linker via  $\gamma$ -butyric acid. To confirm that the ligands specifically bind to CXCR4, a CXCR4–EGFP fusion protein (EGFP = enhanced green fluorescent protein) was transiently expressed in HeLa cells. The increase in binding affinity of the bivalent ligand was clearly reflected in the imaging of CXCR4, as a merged image of TAMRA-labeled **2e** (**6**) and EGFP-fused CXCR4 was observed (Figure 2). When a control monomer, TAMRA-labeled **4** (**7**), was utilized for detection, only a trace of binding was observed. Additionally, binding to mock HeLa cells at the same concentration of ligands was not observed for either ligand (Figure S5).

To further evaluate the binding specificity and dependence on CXCR4 expression levels, fluorescence-activated cell sorting (FACS) analyses utilizing Jurkat, K562, and HeLa cells were performed (Figure 3). The cells were adopted on the basis of their different levels of CXCR4 expression (Jurkat > HeLa > K562).<sup>13</sup> The binding was evaluated by changes in mean fluorescence intensity (MFI) of the above cells in the presence and absence of ligands. The bivalent ligand **6** showed intense binding to Jurkat cells, which highly express CXCR4, as evidenced by the 2.3- and 3.3-fold increases in MFI at 25 and 250 nM, respectively. For binding to HeLa cells, the MFI was increased 2.4-fold by binding

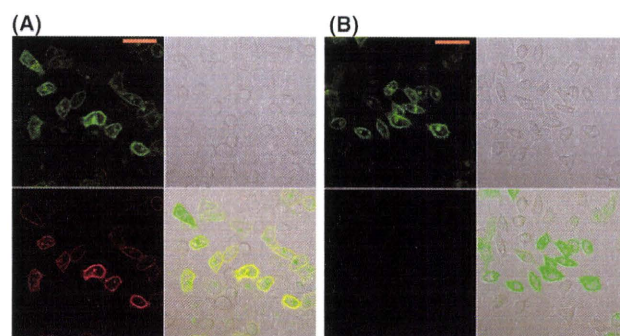


**Figure 2.** Binding of TAMRA-labeled FC131-derived monovalent and bivalent ligands to EGFP–CXCR4-transfected HeLa cells. Bivalent ligand **6** with an optimized linker length was utilized. The pictures show the binding of (A) **6** (25 nM) and (B) **7** (50 nM). Each panel is divided into four sections as follows: upper left, EGFP emission; upper right, differential interference contrast (DIC) image; lower left, TAMRA emission conjugated to ligands; lower right, merged image. Orange bars in the panels represent 50  $\mu$ m.

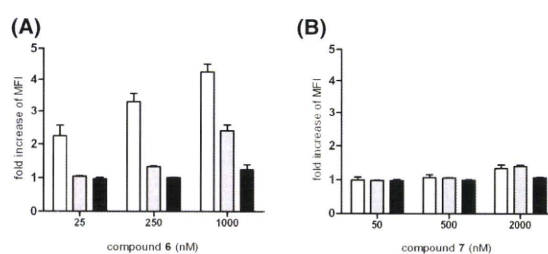


**Figure 3.** FACS analysis to evaluate the dependence of ligand binding on the levels of CXCR4 expression. The columns show the binding of (A) **6** and (B) **7** to Jurkat (white), HeLa (gray), and K562 (black) cells. The fold increase values were calculated by dividing the MFIs of the above cells in the presence of ligands by the corresponding values in the absence of ligands. The results are means of three independent experiments; error bars indicate standard errors of the mean.

of ligand **6** at 1  $\mu$ M, although no significant increase in MFI was observed at 25 or 250 nM **6**, which corresponds with the imaging experiment (Figure S5). Meanwhile, the monovalent ligand **7** at 2  $\mu$ M showed similar binding to Jurkat and HeLa cells, involving 1.1- and 1.4-fold increases in MFI, respectively. These results suggest that it is difficult to distinguish the expression level of CXCR4 by molecular imaging using the monovalent ligand. On the other hand, it is of special interest that the bivalent ligand showed distinguishability of the differences in CXCR4 expression levels. Furthermore, the binding of our CXCR4 ligands would be responsive to CXCR4, as no binding of either ligand to K562 cells, which express a trace of CXCR4, was observed. These results provide evidence in support of the hypothesis that the bivalent ligand binds preferentially to the constitutive dimer of CXCR4. Molecular imaging of CXCR4 on the cell surface by specific antibodies, such as c8352<sup>14</sup> or the monomer ligand T140,<sup>15</sup> has been previously reported. In the present system, however, it is possible that the bivalent ligands could distinguish the density of CXCR4 on the cell surface.

To further assess whether our bivalent ligand could distinguish between cancerous and normal cells by the imaging method, A549 and Human Umbilical Vein Endothelial Cells (HUVEC) were employed for staining as adhesive cell lines. A549 cells are human lung adenocarcinoma human alveolar basal epithelial cells, which are known to possess high CXCR4 expression levels.<sup>16</sup> HUVEC were chosen as a normal cell line without CXCR4 expression. It has been reported that the expression of CXCR4 on HUVEC is induced by fibroblast growth factor (FGF), which is highly expressed in the embryonic stage.<sup>17</sup> Thus, HUVEC was cultured

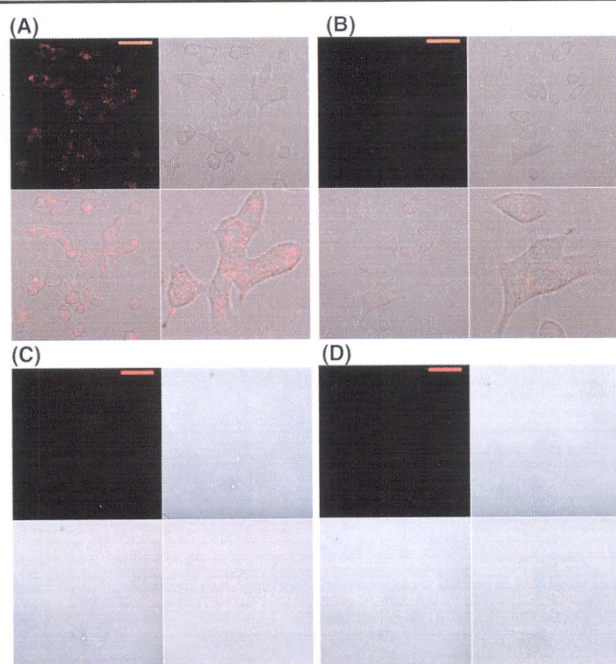


**Figure 4.** Imaging of CXCR4 by TAMRA-labeled FC131-derived monovalent and bivalent ligands on cancerous and normal primary cells. The panels show the binding of (A) **6** (1  $\mu$ M) and (b) **7** (2  $\mu$ M) to A549 cells and (C) **6** (250 nM) and (D) **7** (500 nM) to HUVEC cells. Each panel is divided into four sections as follows: upper left, TAMRA emission image; upper right; DIC image; lower left, merged image; lower right, focused image. Orange bars in the panels represent 50  $\mu$ m.

in the absence of FGF. Ligand **6** showed clear binding to A549 cells (Figure 4A) but not to HUVEC (Figure 4C) at concentrations of 1  $\mu$ M and 250 nM, respectively. On the other hand, monomer ligand **7** showed a trace of binding to each cell line (Figure 4B,D). Bivalent ligand **6** showed binding to HUVEC cultured with FGF at 250 nM (Figure S7). Thus, the bivalent ligands can detect cancerous cells that are in a state of high CXCR4 expression in a specific manner.

In summary, we have presented experimental results concerning the elucidation of the native state of the CXCR4 dimer utilizing bivalent ligands. These lead to a more precise understanding of the oligomerization state. Such a “molecular ruler” approach could be utilized in the design of bivalent ligands for any GPCR. It has been suggested that several GPCRs also exist as heterodimer forms, and CXCR4 has been hypothesized to form heterodimers with CCR2,<sup>18</sup> CCR5,<sup>19</sup> CXCR7,<sup>4b</sup> and the  $\delta$ -opioid receptor.<sup>20</sup> Although the biological significance of GPCRs in homo- or heterooligomerization is still unclear and controversial, the approach described here involving rigid linkers conjugated to ligands specific to each GPCR would lead to elucidation of these issues. Furthermore, through the avidity shown as the specific binding affinity for the dimeric form of CXCR4, the fluorescent-labeled bivalent ligands have been shown to be powerful tools for cancer diagnosis on the basis of their ability to distinguish the density of CXCR4 on the cell surface. Our approach has the advantages that the ligand can directly capture dimeric forms of GPCRs and that the linkers can be applied to virtually any known GPCR.

**Acknowledgment.** The authors thank Prof. Kazunari Akiyoshi (Tokyo Medical and Dental University) for access to the laser scanning microscope. T.T. was supported by JSPS Research Fellowships for Young Scientists. This research was supported in part by New Energy and Industrial Technology Development Organization (NEDO).

**Supporting Information Available:** Curve-fitting data for the binding analyses, CD spectra, docking study of bivalent ligand binding, imaging analyses of mock cells, histogram and MFI of FACS analysis, imaging analyses of HeLa cells cultured with FGF, experimental procedures, and spectral and analytical data for all new compounds. This material is available free of charge via the Internet at <http://pubs.acs.org>.

## References

- (1) Overington, J. P.; Al-Lazikani, B.; Hopkins, A. L. *Nat. Rev. Drug. Discovery* **2006**, *5*, 993–996.
- (2) Wang, J.; He, L.; Combs, C. A.; Roderiquez, G.; Norcross, M. A. *Mol. Cancer Ther.* **2006**, *5*, 2474–2483.
- (3) Percherancier, Y.; Berchiche, Y. A.; Slight, I.; Volkmer-Engert, R.; Tamamura, H.; Fujii, N.; Bouvier, M.; Heveker, N. *J. Biol. Chem.* **2005**, *280*, 9895–9903.
- (4) (a) Babcock, G. J.; Farzan, M.; Sodroski, J. *J. Biol. Chem.* **2003**, *278*, 3378–3385. (b) Luker, K. E.; Gupta, M.; Luker, G. D. *FASEB J.* **2009**, *23*, 823–834.
- (5) (a) Handl, H. L.; Sankaranarayanan, R.; Josan, J. S.; Vagner, J.; Mash, E. A.; Gillies, R. J.; Hruby, V. J. *Bioconjugate Chem.* **2007**, *18*, 1101–1109. (b) Zheng, Y.; Akgün, E.; Harikumar, K. G.; Hopson, J.; Powers, M. D.; Lunzer, M. M.; Miller, L. J.; Portoghese, P. S. *J. Med. Chem.* **2009**, *52*, 247–258.
- (6) Panetta, R.; Greenwood, M. T. *Drug Discovery Today* **2008**, *13*, 1059–1066.
- (7) (a) Tamamura, H.; Xu, Y.; Hattori, T.; Zhang, X.; Arakaki, R.; Kanbara, K.; Omagari, A.; Otaka, A.; Ibuka, T.; Yamamoto, N.; Nakashima, H.; Fujii, N. *Biochem. Biophys. Res. Commun.* **1998**, *253*, 877–882. (b) Fujii, N.; Oishi, S.; Hiramatsu, K.; Araki, T.; Ueda, S.; Tamamura, H.; Otaka, A.; Kusano, S.; Terakubo, S.; Nakashima, H.; Broach, J. A.; Trent, J. O.; Wang, Z.; Peiper, S. C. *Angew. Chem., Int. Ed.* **2003**, *42*, 3251–3253. (c) Tamamura, H.; Araki, T.; Ueda, S.; Wang, Z.; Oishi, S.; Esaka, A.; Trent, J. O.; Nakashima, H.; Yamamoto, N.; Peiper, S. C.; Otaka, A.; Fujii, N. *J. Med. Chem.* **2005**, *48*, 3280–3289. (d) Tanaka, T.; Tsutsumi, H.; Nomura, W.; Tanabe, Y.; Ohashi, N.; Esaka, A.; Ochiai, C.; Sato, J.; Itotani, K.; Murakami, T.; Ohba, K.; Yamamoto, N.; Fujii, N.; Tamamura, H. *Org. Biomol. Chem.* **2008**, *6*, 4374–4377.
- (8) (a) Arora, P. S.; Ansari, A. Z.; Best, T. P.; Ptashne, M.; Dervan, P. B. *J. Am. Chem. Soc.* **2002**, *124*, 13067–13071. (b) Sato, S.; Kwon, Y.; Kamisuki, S.; Srivastava, N.; Mao, Q.; Kawazoe, Y.; Uesugi, M. *J. Am. Chem. Soc.* **2007**, *129*, 873–880.
- (9) (a) Kuemin, M.; Schweizer, S.; Ochsenfeld, C.; Wennemers, H. *J. Am. Chem. Soc.* **2009**, *131*, 15474–15482. (b) Schuler, B.; Lipman, E. A.; Steinbach, P. J.; Kumke, M.; Eaton, W. A. *Proc. Natl. Acad. Sci. U.S.A.* **2005**, *102*, 2754–2759.
- (10) For synthesis details, see the Supporting Information.
- (11) Våbenø, J.; Nikiforovich, G. V.; Marshall, G. R. *Chem. Biol. Drug Des.* **2006**, *67*, 346–354.
- (12) Balkwill, F. *Semin. Cancer Biol.* **2004**, *14*, 171–178.
- (13) (a) Carnec, X.; Quan, L.; Olson, W. C.; Hazan, U.; Dragic, T. *J. Virol.* **2005**, *79*, 1930–1933. (b) Majka, M.; Rozmyslowicz, T.; Honczarenko, M.; Ratajczak, J.; Wasik, M. A.; Gaulton, G. N.; Ratajczak, M. *Z. Leukemia* **2000**, *14*, 1821–1832.
- (14) Schwartz, V.; Lue, H.; Kraemer, S.; Korbil, J.; Krohn, R.; Ohl, K.; Bucala, R.; Weber, C.; Bernhagen, J. *FEBS Lett.* **2009**, *583*, 2749–2757.
- (15) Nomura, W.; Tanabe, Y.; Tsutsumi, H.; Tanaka, T.; Ohba, K.; Yamamoto, N.; Tamamura, H. *Bioconjugate Chem.* **2008**, *19*, 1917–1920.
- (16) Murdoch, C.; Monk, P. N.; Finn, A. *Immunology* **1999**, *98*, 36–41.
- (17) Salcedo, R.; Wasserman, K.; Young, H. A.; Grimm, M. C.; Howard, O. M. Z.; Anver, M. R.; Kleinman, H. K.; Murphy, W. J.; Oppenheim, J. *J. Am. J. Pathol.* **1999**, *154*, 1125–1135.
- (18) Sohy, D.; Parmentier, M.; Springael, J. *J. Biol. Chem.* **2007**, *282*, 30062–30069.
- (19) Contento, R. L.; Molon, B.; Boularan, C.; Pozzan, T.; Manes, S.; Marullo, S.; Viola, A. *Proc. Natl. Acad. Sci. U.S.A.* **2008**, *105*, 10101–10106.
- (20) Pello, O. M.; Martínez-Muñoz, L.; Parrillas, V.; Serrano, A.; Rodríguez-Frade, J. M.; Toro, M. J.; Lucas, P.; Monterrubio, M.; Martínez-A, C.; Mellado, M. *Eur. J. Immunol.* **2008**, *38*, 537–549.

JA107447W

# Development of Crosslink-Type Tag-Probe Pairs for Fluorescent Imaging of Proteins

Wataru Nomura, Tomoaki Mino, Tetsuo Narumi, Nami Ohashi, Akemi Masuda, Chie Hashimoto, Hiroshi Tsutsumi, Hirokazu Tamamura

*Institute of Biomaterials and Bioengineering, Tokyo Medical and Dental University, Chiyoda-ku, Tokyo 101-0062, Japan*

Received 29 January 2010; revised 15 March 2010; accepted 23 March 2010

Published online 4 August 2010 in Wiley Online Library (wileyonlinelibrary.com). DOI 10.1002/bip.21444

## ABSTRACT:

Useful methods of protein labeling via functional peptide tags have been developed in the field of proteome and chemical biology. New tag-probe pairs based on leucine zipper peptides for labeling target proteins are described. These consist of an  $\alpha$ -helical probe peptide with an environmental-sensitive fluorescent dye and two antiparallel  $\alpha$ -helical tag peptides, and may be crosslinked, from the Cys residue of the tag peptide to the  $N^\alpha$ -chloroacetyl group of the probe peptide. Binding of the probe peptide to the tag peptides results in movement of the fluorophore from a hydrophilic to a hydrophobic environment inside the leucine zipper structure, causing a dramatic fluorescent change, mediated by the binding of the two peptides. As a spacer between the  $N^\alpha$ -chloroacetyl group and the original probe sequence, a single Gly residue was the most suitable among 0-2 Gly residues. Crosslinking leads to superior fluorescence response, binding affinity, and chemical stability. These ZIP tag-probe pairs are useful for labeling and fluorescent imaging of proteins. © 2010 Wiley Periodicals, Inc. *Biopolymers (Pept Sci)* 94: 843-852, 2010.

**Keywords:** crosslinking; environmental-sensitive fluorescent dye; fluorogenic tag-probe pair; leucine zipper; protein imaging

This article was originally published online as an accepted preprint. The "Published Online" date corresponds to the preprint version. You can request a copy of the preprint by emailing the Biopolymers editorial office at [biopolymers@wiley.com](mailto:biopolymers@wiley.com)

## INTRODUCTION

In the post-genome era, artificial peptide tools have been used in the field of proteome and chemical biology. In the fluorescent imaging of proteins in living systems, several pairs of peptide tags and their complementary probes have been found to be useful tools. Short peptides which include an oligohistidine tag (His tag) can be incorporated into target proteins and then applied to the purification of recombinant proteins and immobilization of proteins on plates with their complementary molecules, such as the Ni(II)-nitrilotriacetic acid complex (Ni(II)-NTA).<sup>1,2</sup> A His tag has been utilized for fluorescent imaging of proteins in cells using Ni(II)-NTA derivatives with an appended fluorophore.<sup>3-5</sup> In addition, pairs of tetracysteine motif peptides and biarsenical molecular probes, which specifically bind to a tetracysteine sequence, are useful in the real-time fluorescent imaging of cellular proteins.<sup>6,7</sup> Other pairs of short tag peptides and their specific ligands have also been reported.<sup>8-11</sup> A variety of engineered protein tags such as the SNAP tag and the Halo tag have been also reported to be useful in the fluorescent imaging of proteins,<sup>12-15</sup> but in these cases a washing step to remove excess probe molecules, which do not bind to the tag, is required to avoid their background emission. The binding of probes to target proteins via their complementary tags is accompanied by a drastic shift of fluorescent wavelength and/or an increase of fluorescence intensity, facilitating distinction of the labeled proteins and the free probes. Thus, further development of such novel fluorogenic tag-probe pairs is useful and desirable.

Leucine zipper peptides involving three  $\alpha$ -helical antiparallel strands have been utilized as tags for the affinity purifi-

Correspondence to: Hirokazu Tamamura; e-mail: [tamamura.mr@tmd.ac.jp](mailto:tamura.mr@tmd.ac.jp)  
Contract grant sponsors: Ministry of Education, Culture, Sports, Science and Technology, Japan, the Japan Health Science Foundation  
©2010 Wiley Periodicals, Inc.

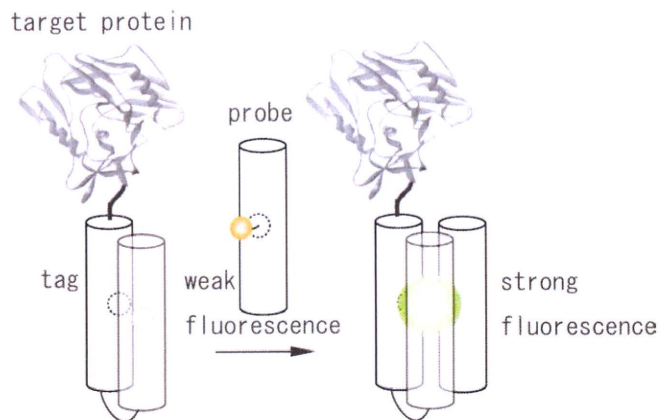


**FIGURE 1** Formation of tag-probe pairs with fluorogenic activity based on the artificial leucine zipper peptides, designated as ZIP tag-probe pairs, and their application to the fluorescent imaging of ZIP tag-fused proteins.

cation of recombinant proteins<sup>16</sup> and as anchors for the immobilization of proteins on micro plates.<sup>17</sup> Complementary selectivity and strong binding affinity have prompted application of new tag-probe pairs to the bio-imaging of proteins. Since hydrophobic cores of leucine zipper peptides can be adjusted to form hydrophobic pockets in which small molecules can bind,<sup>18,19</sup> selective binding of environmentally sensitive fluorescent dyes to these pockets inside the leucine zipper assembly might lead to colorimetric changes and enhance their fluorescence intensity. Accordingly, we have developed new tag-probe pairs with fluorogenic activity based on the artificial leucine zipper peptides, designated as ZIP tag-probe pairs, and applied them to the fluorescent imaging of ZIP tag-fused protein on the surface of living cells (see Figure 1).<sup>20</sup>

The design of ZIP tag-probe pairs was based on the crystal structure of an antiparallel coiled-coil trimer of a GCN4 mutant shown in Figure 2.<sup>21</sup> A probe peptide consists of an  $\alpha$ -helical peptide in which 4-nitrobenzo-2-oxa-1,3-diazole (NBD), an environmentally sensitive fluorescent dye is imbedded. The NBD is attached to the side chain of the

L- $\alpha$ -2,3-diaminopropionic acid residue (Dap(NBD)) at position 13 on the hydrophobic site of the leucine zipper structure. A tag peptide consists of antiparallel 2  $\alpha$ -helical peptides linked via a Gly-Gly-Cys-Gly-Gly loop sequence. Two Leu residues in the tag peptide, located at the positions complementary to the Dap(NBD) residue of the probe peptide, are replaced by Ala so that an adequate hydrophobic pocket is formed when the tag peptide binds to the probe peptide.

In fluorescent titration analysis, the change in the fluorescence spectra of the probe peptide depends largely on the concentration of the tag peptide. The emission spectra derived from NBD showed a 17-fold increase in emission intensity with a concomitant blue shift of the emission maximum from 535 nm to 505 nm (see Figure 3). This spectral change shows that the NBD moiety of the probe peptide is located in the hydrophobic environment inside the 3 $\alpha$ -helical peptide bundle structure. The dissociation constant of the probe peptide toward the tag peptide, was estimated by analysis of the fluorescent titration curve with a nonlinear least-squares curve fitting method<sup>22</sup> at 18 nM. The tag-probe pair was also applied to the fluorescent imaging of the tag-fused CXCR4 by the probe peptide in the living cells. CXCR4 is a member of a chemokine receptor family, involving seven transmembrane G-protein coupled receptor (7TM-GPCR) families.<sup>23,24</sup> The tag-fused CXCR4, in which the tag is genetically fused to the extracellular N-terminus region of CXCR4, is transiently expressed on the surface of CHO-K1 cells. Sequential labeling experiments of the tag-fused CXCR4 using the probe peptide with the NBD dye and a fluorescent CXCR4 antagonist were performed. In the presence of the excess probe peptide, the labeling of tag-fused CXCR4 using the probe peptide with NBD produced bright green fluorescence on the surface of the cells (see Figure 4).<sup>25</sup> Subsequently, the tag-fused CXCR4 was stained in a red color by the CXCR4 antagonist, tetramethylrhodamine (TAMRA)-appended T140. In this way, a membrane protein CXCR4 can be successfully visualized using the ZIP tag-probe system which this is shown to be a useful fluorescent imaging tool for proteins in living cells. The tag-probe complex consist-

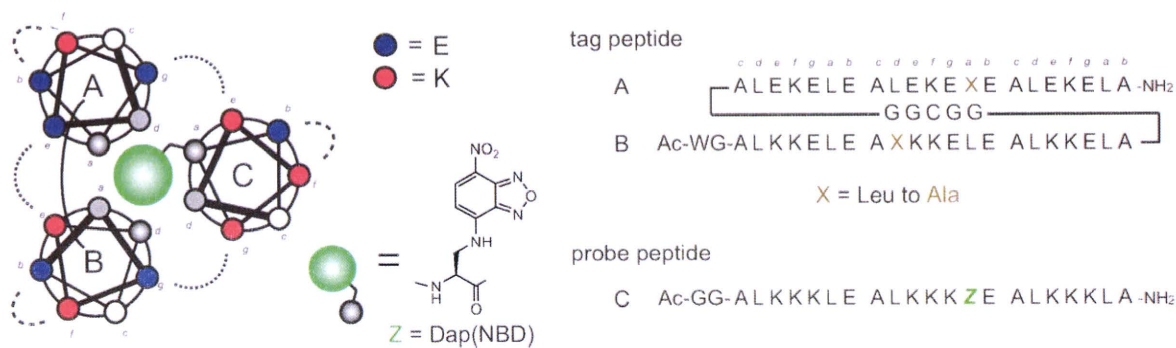


**FIGURE 2** Design and structure of ZIP tag-probe pairs.

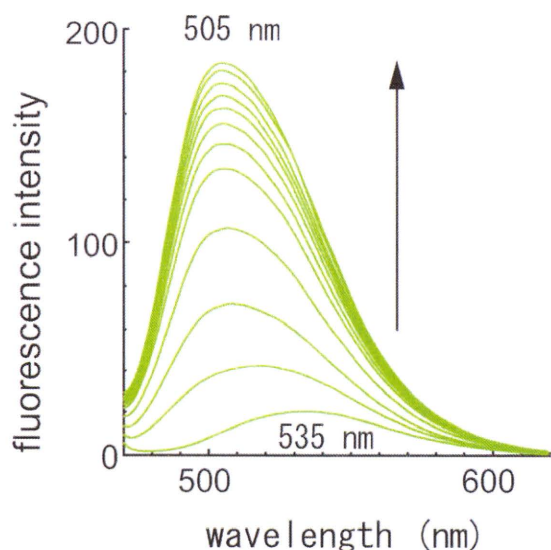


**FIGURE 3** Fluorescence spectral change of the probe peptide upon the addition of the tag peptide at 25 °C in 50 mM HEPES buffer (pH 7.2, 100 mM NaCl): [probe] = 0.5  $\mu$ M, [tag] = 0 to 2.0  $\mu$ M.

ing of the antiparallel  $3\alpha$ -helical peptide bundle structure is formed as a result of the affinity of the tag peptide and the probe peptide. Since this interaction involves noncovalent bonds, introduction of crosslink by a covalent bond might increase chemical and biological stability. Thus, we developed tag-probe pairs, crosslinked by covalent bonds (see Figure 5).

## RESULTS AND DISCUSSTION

### Crosslinking Reaction of the Tag Peptide With the Probe Peptide

To investigate the optimum length of crosslinkers, three types of probe peptides with linkers of different lengths were synthesized. The original tag peptide has a side-chain thiol group in the Gly-Gly-Cys-Gly-Gly loop structure between

antiparallel  $2\alpha$ -helical peptides. At the N-terminus of each probe peptide, 0, 1, or 2 Gly residues were attached as a spacer and an N<sup>z</sup>-chloroacetyl group as a functional group for coupling with the Cys thiol group (see Figure 6). The probe peptides having 0, 1, and 2 Gly residues were designated probe 1, 2, and 3. As control probe peptides, probe peptide 4, which has no chloroacetyl group, and 5, which has N<sup>z</sup>-chloroacetyl-Lys at the C-terminus, both possessing N<sup>z</sup>-acetyl-Gly, were also prepared. Probe peptides 1-5 were prepared by Fmoc-based solid-phase peptide synthesis.<sup>26</sup> The tag peptide was prepared by native chemical ligation<sup>27,28</sup> of the synthetic C-terminal thioester fragment A and the N-terminal cysteine fragment B, which were divided at the cysteine residue of the loop sequence.<sup>20</sup> Using the probe peptides 1-3, the crosslinking reactions with the tag peptide, monitored by HPLC,<sup>29</sup> were performed by addition of the tag peptide to the probe peptide (1:1, final 1  $\mu$ M each) in 50 mM HEPES buffer, pH 7.2 containing 100 mM NaCl at room temperature. The time course of the crosslinking reaction of the probe peptide 2 is shown in Figures 7 and 8a. Peak areas of the tag peptide and the probe peptide 2 with the retention times of  $\sim$ 18 min and 32 min, respectively, decreased in a time-dependent manner, while that of the product of crosslink, the tag-probe 2 complex, with retention time of 28 min, increased. Completion of this reaction was the fastest of the crosslinking reactions, requiring approximately 20 min (Figure 8b). The order of the reaction rate of the probe peptides was 2, 1, 3, and 5 (Figures 8b and 9). Reactions of 1 and 3 were mostly complete in 30 min, and the crosslinking reaction of the tag peptide with the probe peptide 5 failed (see Figure 9). These results suggest that a Gly residue at position 1 is the most suitable spacer and that the chloroacetyl group of the probe peptide and the thiol group of the tag peptide react in a structure-specific manner. In the use of the probe peptides 1-3 to form the tag-probe pairs, the chloroacetyl and thiol groups approach one another prior to the cross-

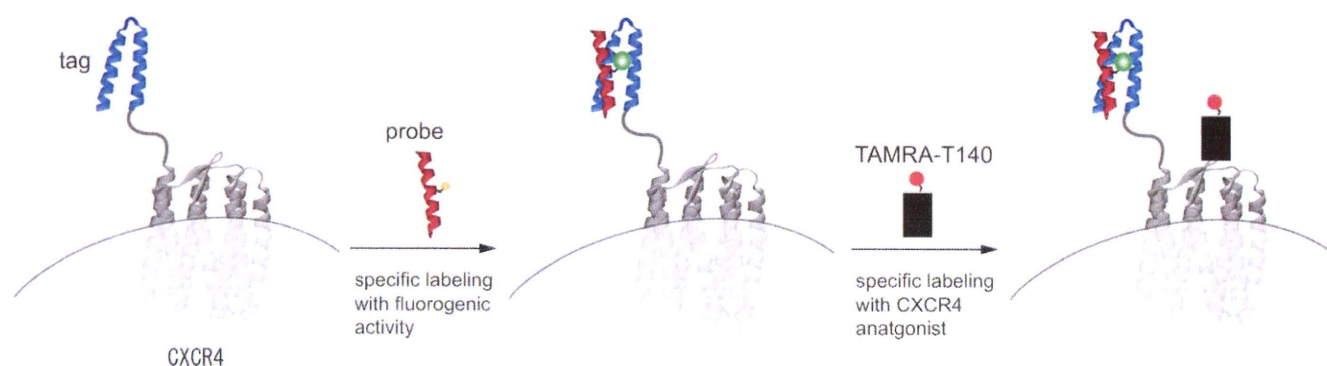


**FIGURE 4** Sequential labeling of the tag-fused CXCR4 on the cell surface by the TAMRA-appended CXCR4 antagonist T140 after the labeling by the probe peptide.



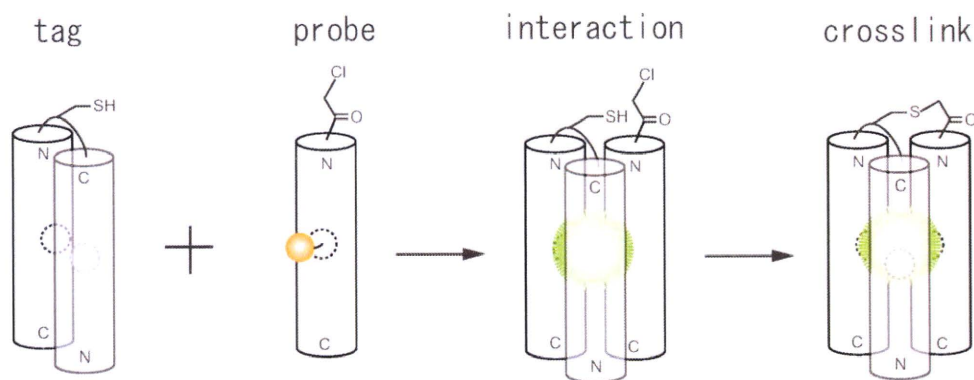


**FIGURE 5** Crosslink-type ZIP tag-probe pairs with fluorogenic activity; formation of tag-probe pairs and the subsequent crosslink by a covalent bond.

linking reaction. In the case of the probe peptide 5, when the tag-probe pair is formed the chloroacetyl and thiol groups are located quite separately on opposite sides and can not interact. All of the crosslink products were purified by RP-HPLC and characterized by ESI-MS.

### Fluorescent Titration Analysis

In the fluorescent titration analysis of the addition of the tag peptide to the probe peptide 2, the fluorescence spectra of 2 changed remarkably, depending on the concentration of the tag peptide. The emission maximum due to the NBD dye showed a significant blue shift from 537 nm to 504 nm with a 22-fold increase in the emission intensity (see Figure 10). Such a spectral change clearly suggests that the NBD moiety of the probe peptide is located in the hydrophobic environment inside the  $3\alpha$ -helical peptide bundle structure, as in noncovalent type formation of the ZIP tag-probe pair.<sup>20</sup> Comparison with the other probe peptides in the fluorescent

titration analysis is shown in Figure 10b and Table I. In the use of all of the probe peptides, a similar blue shift of the emission maximum due to the NBD dye from 534–537 nm to 504 nm was observed. The increase of emission intensity, most remarkable in the case of probe peptide 2, was in the order 2, 1, 3, 4, and 5. This suggests that tag-probe 2 pair is most suitable for analytical purposes.

The dissociation constants of the probe peptides 1, 2, 3, 4, and 5 toward the tag peptide were estimated by analysis using nonlinear least-squares curve fitting<sup>22</sup> as 6.2 nM, 6.5 nM, 9.0 nM, 22 nM, and 12 nM, respectively (Table I). Thus, in terms of dissociation constant, the probe peptide 1 is comparable to 2, indicating similar binding affinities, but the hydrophobic environment formed by the interaction of the tag peptide with the probe peptide 2 would appear to be more suitable for the fluorescence emission of the NBD dye.

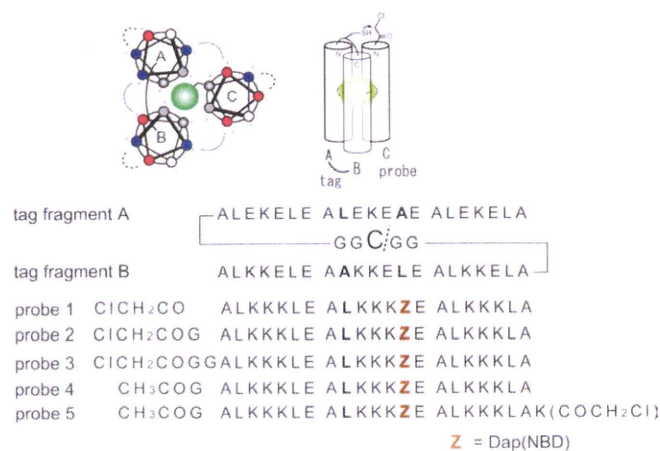


**FIGURE 6** Design and structure of crosslink-type ZIP tag-probe pairs. Probe peptides 1–3 have an N<sup>α</sup>-chloroacetyl group at the N-terminus. Probe peptides 4 and 5 have an N<sup>α</sup>-acetyl group at the N-terminus. Probe peptide 5 has N<sup>ε</sup>-chloroacetyl-Lys at the C-terminus.

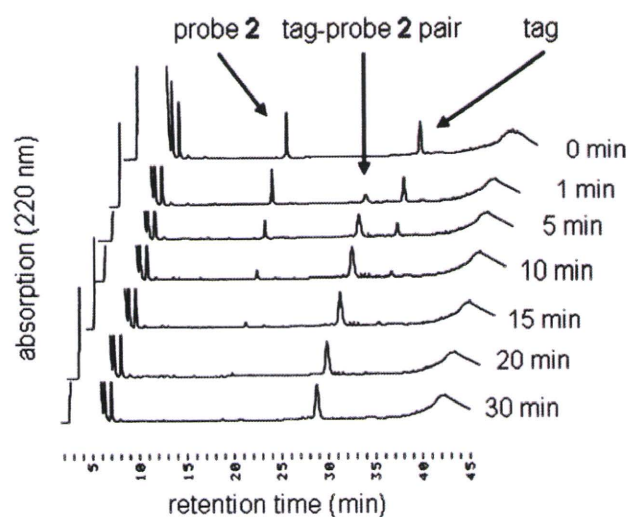


**FIGURE 7** HPLC monitoring of the crosslinking reaction of the tag peptide with the probe peptide 2. The reaction was performed by addition of the tag peptide to the probe peptide 2 (1:1, final 1  $\mu$ M each) in 50 mM HEPES buffer, pH 7.2 containing 100 mM NaCl at room temperature.

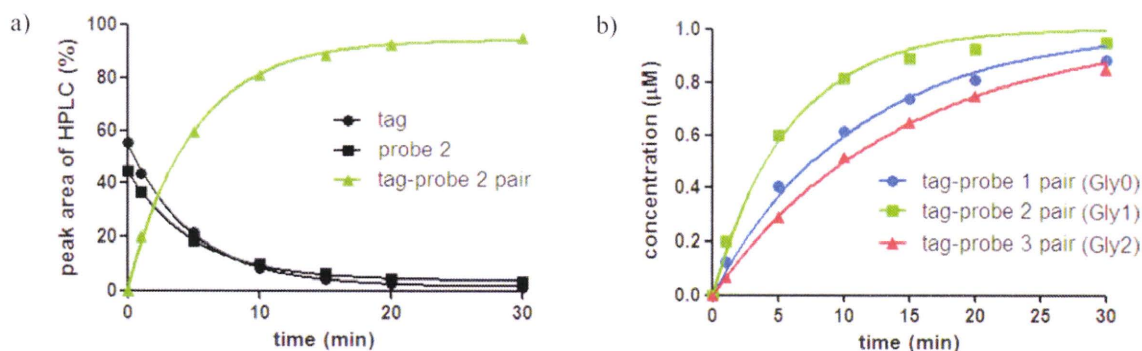


FIGURE 8 The time course of the crosslinking reaction of the tag peptide with the probe peptides. (a) The time course of HPLC peak areas of tag, probe 2 and tag-probe 2 pair, (b) the time course of concentrations of resulting tag-probe 1-3 pairs.

Compared with the noncovalent tag-probe 4 pair, whose dissociation constant is 22 nM, the affinities of the covalent type tag-probe 1, 2, and 3 pairs are remarkably higher, suggesting that crosslink of tag and probe peptides underlies the increase in affinity. In the tag-probe 5 pair, a similar spectral change was observed, indicating that the NBD dye was located in the hydrophobic pocket, although a covalent bond for crosslink of tag and probe peptides was apparently absent (see Figure 11).

### Fluorescence Job's Titration

Fluorescent Job's titration, recording the intensity at 505 nm, was performed to assess the stoichiometry of the tag-probe 2 complex (see Figure 12). The total concentration of the probe peptide 2 and the tag peptide was fixed at 1.0 μM. The concentrations of the tag peptide were 0, 0.2, 0.4, 0.5, 0.6, 0.8, and 1.0 μM. This fluorescence Job's titration experiment clearly indicates that the probe peptide 2 binds to the tag peptide

with 1:1 stoichiometry. The result suggests that the tag peptide and the probe peptides 1-3 form a stable 3 $\alpha$ -helical leucine zipper structure by binding with 1:1 stoichiometry.

### Investigation of Chemical Stability by Fluorescence Analysis

The chemical stability to thermal denaturation of the tag-probe complexes was investigated. Using the complexes of the tag peptide and the probe peptides 1-5, changes of fluorescence intensity were monitored. The aqueous solution of 1 μM tag-probe complex in 50 mM HEPES buffer, pH 7.2 containing 100 mM NaCl was prepared, and then the temperature of the solution was gradually increased to 100°C. Fluorescence spectral changes of the tag-probe peptide 2 and 4 pairs, representatives of crosslink pairs and noncrosslink pairs, are shown in Figure 13. In Figure 14 changes of fluorescence intensity of the tag-probe peptide 1-5 pairs are shown. In each of the complexes of the tag peptide with probe peptides 1-5, a gradual

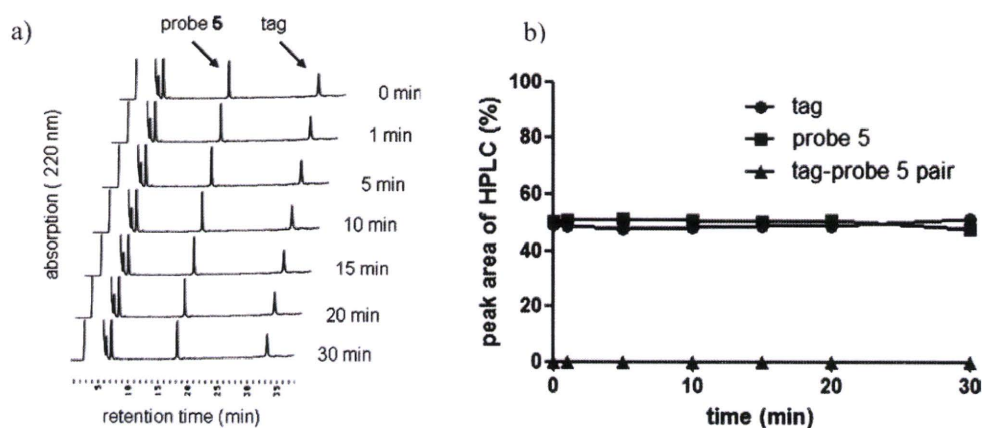


FIGURE 9 (a) HPLC monitoring of the crosslinking reaction of the tag peptide with the probe peptide 5. The reaction was performed by addition of 1 μM tag peptide to 1 μM probe peptide 5 in 50 mM HEPES buffer, pH 7.2 containing 100 mM NaCl at room temperature. (b) The time course of HPLC peak areas of tag, probe 5 and tag-probe 5 pair.

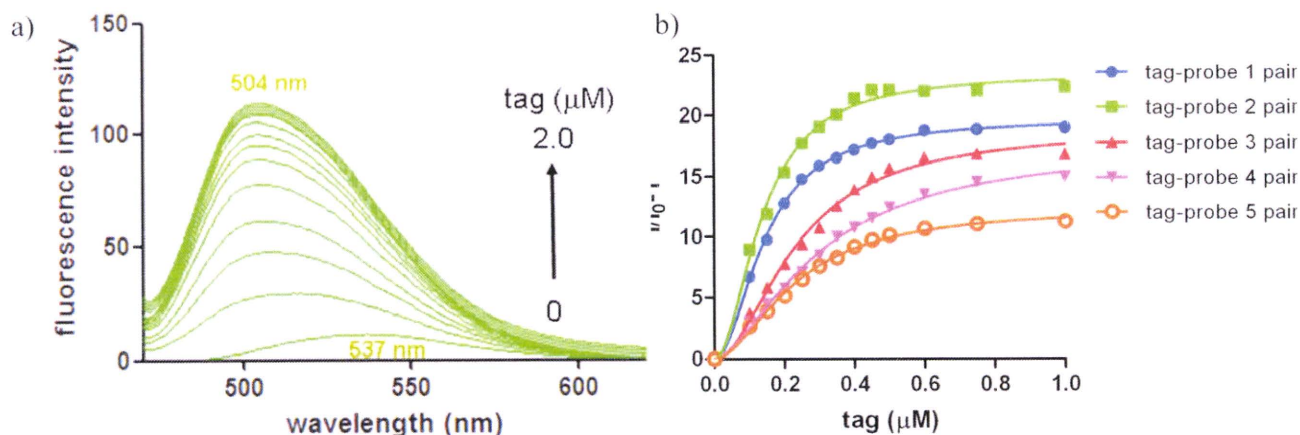


FIGURE 10 (a) Fluorescence spectral change of the probe peptide 2 upon the addition of the tag peptide at 25 °C in 50 mM HEPES buffer (pH 7.2, 100 mM NaCl): [probe] = 0.5  $\mu$ M, [tag] = 0 to 2.0  $\mu$ M. (b) Change of fluorescence intensity of the probe peptides 1-5 upon the addition of the tag peptide for calculation of dissociation constants of tag-probe pairs.

decrease in fluorescence intensity was observed in proportion to the increase of temperature. The complexes of the tag peptide and the probe peptides 1-3 were more stable than those of 4 and 5, which were completely denatured at 100 °C, but the complexes using 1-3 were not denatured, possibly due to the crosslinking. The melting temperatures of the complexes using 1-3 were above 69 °C, whereas those of the complexes involving 4 and 5 were below 56 °C.

The possibility that this thermal denaturation is reversible was next investigated. The pairs of tag-probe 2 and tag-probe 4 were adopted as representative of crosslink pairs and non-crosslink pairs, respectively. After denaturing the tag-probe 2 pair at 100 °C, the temperature of the solution was gradually decreased (Figure 15a). In proportion to the decrease of temperature, a gradual increase in fluorescence intensity of probe 2 was observed, resulting finally in complete recovery of the original fluorescence intensity. In contrast, while a gradual increase in fluorescence intensity, proportionate to a decrease in temperature, was also observed after the thermal denaturation at 100 °C of tag-probe pair 4, the fluorescence intensity recovered only to

approximately half of its original level (Figure 15b). These results suggest that the crosslinking of tag and probe peptides is critical for complete reversibility of the fluorescence emission.

### Investigation of Chemical Stability by Circular Dichroism

The chemical stability of the tag-probe complexes to thermal denaturation was investigated by circular dichroism (CD). The CD spectra showed that all of the tag-probe 1-4 complexes form  $\alpha$ -helical structures. The CD spectrum of the tag-probe 2 complex had the strongest double minima at 207 and 222 nm, while the spectrum of the non-covalent type tag-probe 4 complex showed the weakest double minima among the four complexes (see Figure 16). This result sug-

Table I Results of Fluorescence Titration of Tag-Probe Pairs

	Fluorescence Wavelength		Dissociation Constant (nM) <sup>a</sup>
	of Emission Maximum (nm)	$I_{\max}/I_0$ (Fold)	
Tag-probe 1 pair	537–504	19	6.2
Tag-probe 2 pair	537–504	23	6.5
Tag-probe 3 pair	535–504	17	9.0
Tag-probe 4 pair	534–504	15	22
Tag-probe 5 pair	534–504	11	12

<sup>a</sup> Measurement conditions: 50 mM HEPES buffer solution (pH 7.2, 100 mM NaCl), at 25 °C, [probe] = 0.5  $\mu$ M.

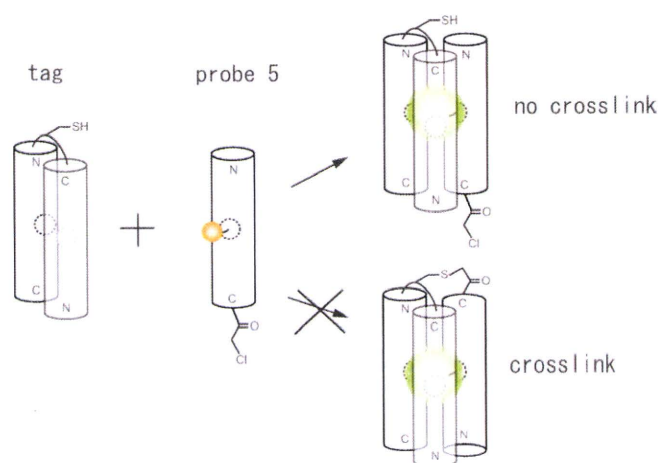


FIGURE 11 Formation of tag-probe 5 pair without crosslinking. When tag-probe 5 pair is formed, the chloroacetyl and thiol groups are separated, located on opposite sides and no covalent bond can form between them.

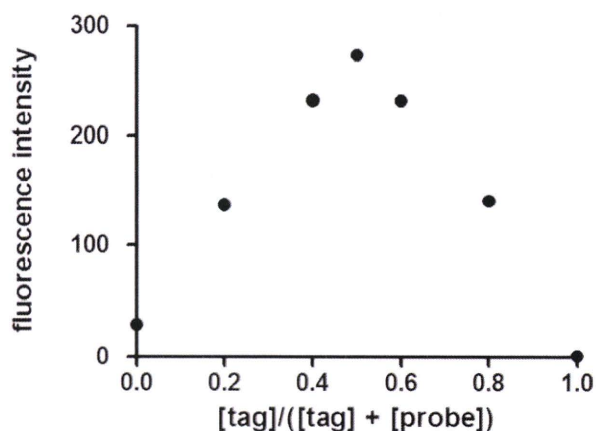


FIGURE 12 Fluorescence Job's titration between the probe peptide 2 and the tag peptide,  $[\text{probe } 2] + [\text{tag}] = 1.0 \mu\text{M}$ , in 50 mM HEPES buffer (pH 7.2, 100 mM NaCl) at 25°C.

gests that crosslinking of the tag and probe peptides is essential for the  $\alpha$ -helical structures. Changes in  $[\theta]$  at 222 nm in aqueous solution of 1  $\mu\text{M}$  tag-probe pair in 50 mM Tris-HCl buffer, pH 7.2 containing 100 mM NaCl were monitored, and the temperature of the solution was gradually increased to 94°C (Figure 17a). In all the tag-probe 1-4 pairs, a gradual increase in values of  $[\theta]$  at 222 nm was observed in proportion to the increase in temperature. Tag-probe 4 pair, in particular, showed a remarkable increase in values of  $[\theta]$  at 222 nm, suggesting that the  $\alpha$ -helical structures were largely collapsed. Judging by the changes of  $[\theta]$  at 222 nm, the  $\alpha$ -helical structures of tag-probe 1-3 pairs survived better than those of tag-probe 4 pair, possibly due to the crosslinking. Next, whether the above  $\alpha$ -helical structures can be reversibly recovered was investigated (Figure 17b). The pairs of the tag peptide and the probe peptides 2 and 4 were adopted as representatives of crosslink pairs and noncrosslink pairs, respectively. After denaturing the tag-probe 2 and 4 pairs at 94°C,

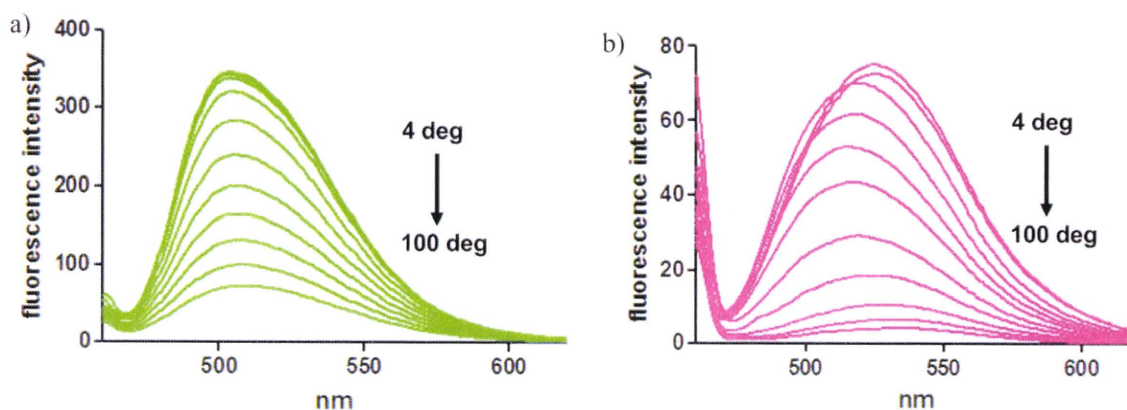


FIGURE 13 Fluorescence spectral change of tag-probe pairs from 4°C to 100°C in 50 mM HEPES buffer (pH 7.2, 100 mM NaCl):  $[\text{tag-probe pair}] = 0.5 \mu\text{M}$ . (a) tag-probe 2 pair, (b) tag-probe 4 pair.

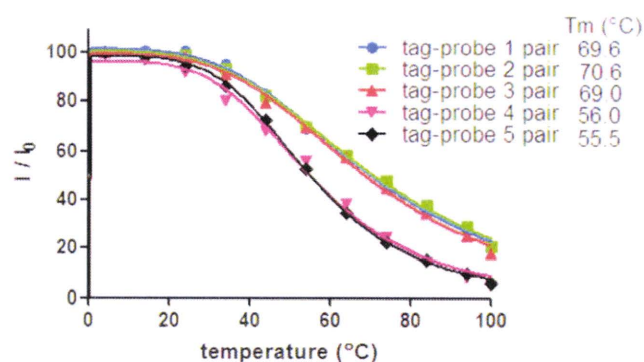


FIGURE 14 Change of fluorescence intensity of tag-probe 1-5 pairs from 4°C to 100°C in 50 mM HEPES buffer (pH 7.2, 100 mM NaCl):  $[\text{tag-probe pair}] = 0.5 \mu\text{M}$ . Values of melting temperature ( $T_m$ ) of tag-probe peptide 1-5 pairs are shown.

the temperature of the solution was gradually decreased, Gradual decreases in values of  $[\theta]$  at 222 nm in proportion to the decrease of temperature were observed with both pairs. In the case of the tag-probe 2 pair the value of  $[\theta]$  at 222 nm was finally nearly completely recovered but with the tag-probe 4 pair  $[\theta]$  was not reduced to its original value, suggesting that the crosslink of tag and probe peptides is indispensable for complete reversibility of the  $\alpha$ -helical structures.

## CONCLUSION

The novel tag-probe pairs based on leucine zipper peptides, in which the thiol group of the Cys residue of the tag peptide and the chloroacetyl group of the probe peptide were crosslinked, have been studied. They were found to have significant fluorogenic activity, mediated by the binding of the tag peptide to the probe peptide as the noncrosslink-type pairs. Compared with noncrosslinked tag-probe pairs, those that are crosslinked were shown to have some advantages in terms of fluorescence